(Y t C ...

UNCLASSIFIED

CLASSIFICATION LEVEL
(S, C OR U)

A. M. PERRY

ATOMICS INTERNATIONAL

AI-AEC-MEMO COVER SHEET

REPORT TITLE **STRUCTURAL ANALYSIS OF THE SNAP 8 DEVELOPMENTAL REACTOR FUEL ELEMENT CLADDING**

AUTHOR
A. W. Dalcher

AI-AEC-MEMO 12824

(This Document Contains _____ Pages.
This is Copy 1 of ____ Series ____)

NOTICE

PORTIONS OF THIS REPORT ARE ILLEGIBLE.

It has been reproduced from the best available copy to permit the broadest possible availability.

AI-AEC-Memo--12824

TI85 004476

CLASSIFICATION TYPE
(RD OR DI)

MASTER

DISTRIBUTION OF THIS DOCUMENT IS UNLIMITED

UNCLASSIFIED

CLASSIFICATION LEVEL
(S, C OR U)

DO NOT REMOVE THIS SHEET

FORM 759-H-1 REV. 8-68

DISCLAIMER

DISCLAIMER

ATOMICS INTERNATIONAL
A Division of North American Aviation, Inc.

TECHNICAL DATA RECORD

AI-AEC-TDR NO	12824
PAGE	1 OF
DATE	4/15/69
GO NO	7759
S/A NO	13330
TWR	

APPROVALS

R P Jetter 5/19/69

AUTHOR: A. W. Dalcher

DEPT & GROUP NO.: 731-131

TITLE: Structural Analysis of the SNAP-8 Developmental Reactor Fuel Element Cladding

PROGRAM: SNAP-8

SUBACCOUNT TITLE: S8DR Fuel Cladding Stress Analysis

SECURITY CLASSIFICATION

(CHECK ONE BOX ONLY)

	AEC	DOD
UNCL.	☒	☐
CONF.	☐	☐
SECRET	☐	☐

(CHECK ONE BOX ONLY)

RESTRICTED DATA ☐

DEFENSE INFO. ☐

AUTHORIZED CLASSIFIER SIGNATURE: R P Jetter DATE: 5/19/69

DISTRIBUTION

	E. Donovan	BB21
	R. Jetter	BB30
	R. Johnson	BB02
	L. Maki	BB03
	D. Mason	BB02
	G. Meyers	AB02
	D. Nelson	BB29
	T. Parker	AB02
*	W. Roberts	DA01
	H. Rood	BB22
*	R. Varnes	BB14
*	R. Williams	BB13
	R. Wilson	BB01
*	Structural Design Unit (11)	BB30
	A. Dalcher (2)	BB30

STATEMENT OF PROBLEM

Determine the structural adequacy of the S8DR fuel element cladding for the conditions of fabrication, assembly, steady-state, and transient operation.

ABSTRACT

Primary, secondary, and thermal stresses were calculated and evaluated for the SNAP-8 developmental reactor fuel element cladding. The effects of fabrication and assembly stresses, as well as test and operational stresses were included in the analysis. With the assumption that fuel-swelling-induced stresses are nil, the analytical results indicate that the cladding assembly is structurally adequate for the proposed operation.

FORM 701-C REV. 10-62

TABLE OF CONTENTS

I. INTRODUCTION

The SNAP-8 reactor is intended for use as a primary power source on satellites and other space vehicles. The performance objectives of the reactor are: 600 kwt thermal power, 1300°F NaK outlet temperature, 12,000 hour reactor operating period, and greater than 96% reliability.

To demonstrate the accomplishment of these objectives, the SNAP-8 developmental reactor (S8DR) is being constructed as a ground-test prototype of a flight-configured reactor. It is designed for 600 kwt power at 1300°F outlet temperature or, alternately, 1 Mwt at 1100°F outlet. The reactor will be run for a minimum of 12,000 hours.

This report summarizes the results of the analyses and evaluation of mechanical and thermal stresses imposed on the S8DR fuel element cladding during fabrication, assembly, test, and operation. Only the 600 kwt operation has been evaluated, since this power level is more severe from the standpoint of stress evaluation (due to the higher operating temperatures). The conditions considered are consistent with those described in the series of SNAP-8 Program Office briefings: NAA-SR-MEMO-12097, -12122, and -12272 (Ref. I.1, I.2, I.3) and with the detailed core thermal and hydraulic performance report, NAA-SR-12564 (Ref. I.4).

II. DESIGN DESCRIPTION

The reference S8DR fuel element assembly is described by AI Drawing S8DR-18001. The assembly cladding consists of a drawn cylindrical tube with a machined end cap attached at each end. The cladding material is Hastelloy-N, nickel base alloy. A ceramic hydrogen barrier is bonded to the inner surface of the cladding.

REVISIONS			
SYM	DESCRIPTION	DATE	APPROVED
A	1. DELETED GAGE LINE SCHEMATIC & RELATED DIMS FROM DETAIL OF ASSY. ADDED SEPARATE SCHEMATIC & RELATED DIMS TO F/D 2. ADDED TO END OF G/N 6 - WITH .570 DIA ------ FOR LENGTH NOTED 3. .350 REF WAS .335 REF 4. IN G/N 12 DIM .350±.020 WAS .335±.015 5. IN G/N 5 .004 T.I.R. WAS .002 T.I.R. 6. 6.70±.50 WAS 7.50±.50	5/9/67	W. PERRIN

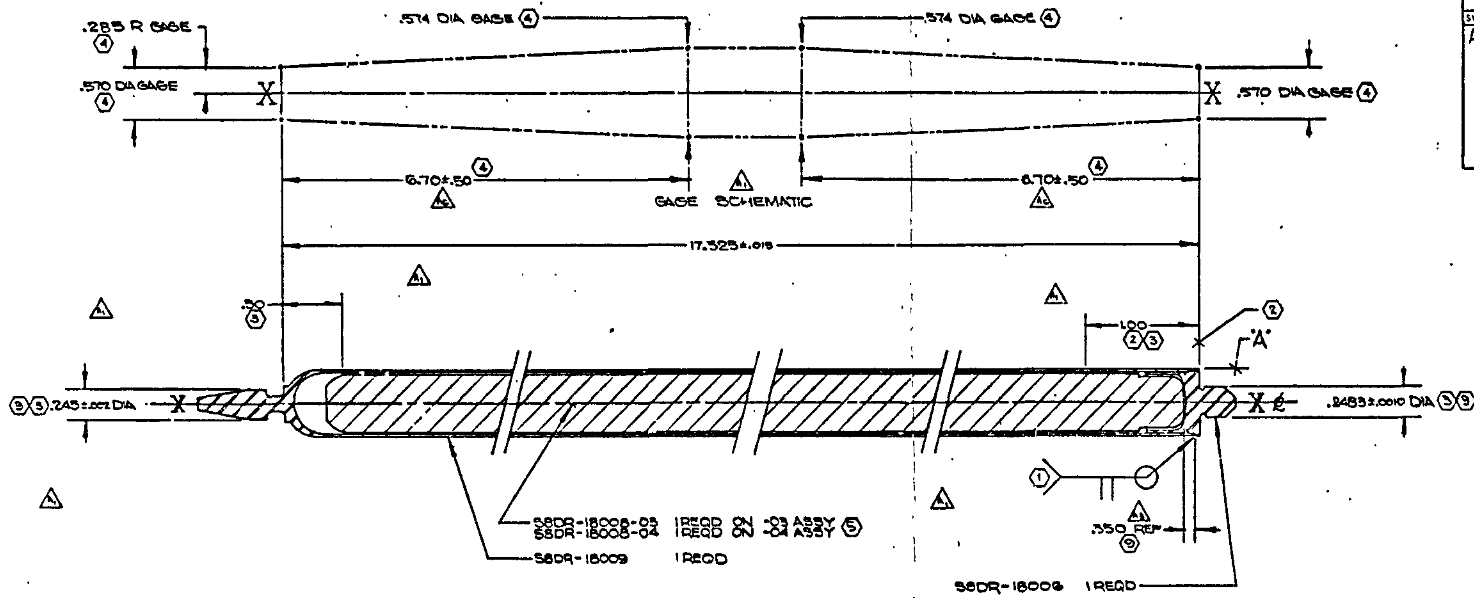

FOR INFORMATION
WILL NOT BE REPLACED AND MAY BE CHANGED WITHOUT NOTICE

⑥ 9. FOR EXPERIMENTAL USE ONLY, QUANTITY REQD TO BE DETERMINED BY PROGRAM OFFICE
⑤ 8. CAUTION! DANGEROUS, UNSTABLE OR TOXIC MATL SPECIAL HANDLING REQD
7. PACKAGE FOR SHIPMENT OR STORAGE PER AI SPEC NA0116-001 UNIT PROTECTION METHOD III
④ 6. EACH FEATURE OF SURFACE NOTED MUST LIE WITHIN A BOUNDARY DEFINED BY GAGE DIA'S SHOWN WITH .570 DIA INCREASING LINEARLY TO .574 DIA FOR LENGTH NOTED

⑨ 12. DURING ASSY OF ELEMENT, AFTER INSERTION OF FUEL ROD (S8DR-18008) INTO TUBE ASSY (S8DR-18009), TAKE DEPTH MEASUREMENT TO ASCERTAIN THAT END OF FUEL ROD IS .350±.020 BELOW OPEN END OF TUBE
⑧ 11. S8DR-18001-4 (ENRICHED & POISONED ASSY) SHALL BE IN ACCORDANCE WITH AI SPEC NES8DR-18-001 TYPE 2
⑦ 10. S8DR-18001-3 (NORMAL & POISONED ASSY) SHALL BE IN ACCORDANCE WITH AI SPEC NES8DR-18-001 TYPE 1

⑤ 5. DIA'S TO BE CONCENTRIC TO CENTER LINE X-X AS ESTABLISHED FROM OD. AT LOCATIONS SHOWN WITHIN .004 T.I.R.
② 4. NORMAL TO SURFACE "A" AS ESTABLISHED IN INDICATED LENGTH WITHIN .004 TOTAL AT LOCATION SHOWN
① 3. ASSEMBLE PER AI SPEC ST 0822 NA 0041
2. CENTER DRILL ON PART NOT PERMISSIBLE
1. FABRICATE PER AI SPEC NA0103-005

NOTES: UNLESS OTHERWISE SPECIFIED

QTY REQD (B)	QTY REQD (1)	QTY REQD	PART OR IDENTIFYING NO	NOMENCLATURE OR DESCRIPTION	CODE IDENT	MATERIAL	DATA, SPECIFICATIONS SIZES, NOTES, VENDORS	LINE NO
1	1		S8DR-18009	TUBE ASSY				005
1			S8DR-18008-04	FUEL ROD				004
	1		S8DR-18008-03	FUEL ROD				003
1	1		S8DR-18006	CUP PLUG				002
-04	-03		S8DR-18001	ASSEMBLY				001

LIST OF MATERIALS OR PARTS LIST

ITEM	QTY	MODEL	NEXT USING DRAWING
-04	(11)	S8DR	S8DS-12002
-03	(G)		

REQD PER END ITEM
APPLICATION (USAGE) DATA

UNLESS OTHERWISE SPECIFIED DIMENSIONS ARE IN INCHES. TOLERANCES ON DECIMALS ANGLES FRACTIONS
XX = ± .03 ±30' ±1/32
XXX = ± .010
HOLES NOTED "DRILL"
.013 THRU .040 : +.001 -.001
.041 THRU .130 : +.002 -.001
.131 THRU .229 : +.003 -.001
.230 THRU .500 : +.004 -.001
.501 THRU .750 : +.005 -.001
.751 THRU 1.000 : +.007 -.001
1.001 THRU 2.000 : +.010 -.001
DO NOT SCALE PRINT

DR BY W. PERRIN 1-25-67
CHK BY 2-6-67
APPROVED BY

ATOMICS INTERNATIONAL
A Division of North American Aviation, Inc.
CANOGA PARK, CALIFORNIA

FUEL ELEMENT ASSEMBLY

CODE IDENT NO 09974 SIZE D S8DR-18001
SCALE 4:1 SHEET

S8DR-18001 A

REDUCED DRAWING

III. OPERATING CONDITIONS

A. Static Loads

1. Operating Pressures

The operating pressures in the fuel element, and in the NaK are given in Table III.A.1.

TABLE III.A.1.
Operating Pressures

Location	Pressure (psia)	
	Beginning-of-Life	End-of-Life
Fuel Element*	15.9 Max.	2.8 - 16.2
NaK System†	35.0	35.0

* Ref. III.A.1.
† S8 Project Management Selected Level

The fuel element pressure is primarily due to hydrogen dissociation from the fuel, and varies with lifetime and element location as shown in Figure III.A.1. The values given in the curve are derived from nominal dissociation and leakage rates. Fission product gas pressure is practically negligible for the design life of the reactor. Values are given in Table III.A.2 which were calculated based on the relationships given in Ref. III.A.2.

FIG. III.A.1.

58DS FUEL ELEMENT HYDROGEN PRESSURE (NOMINAL PREDICTED)

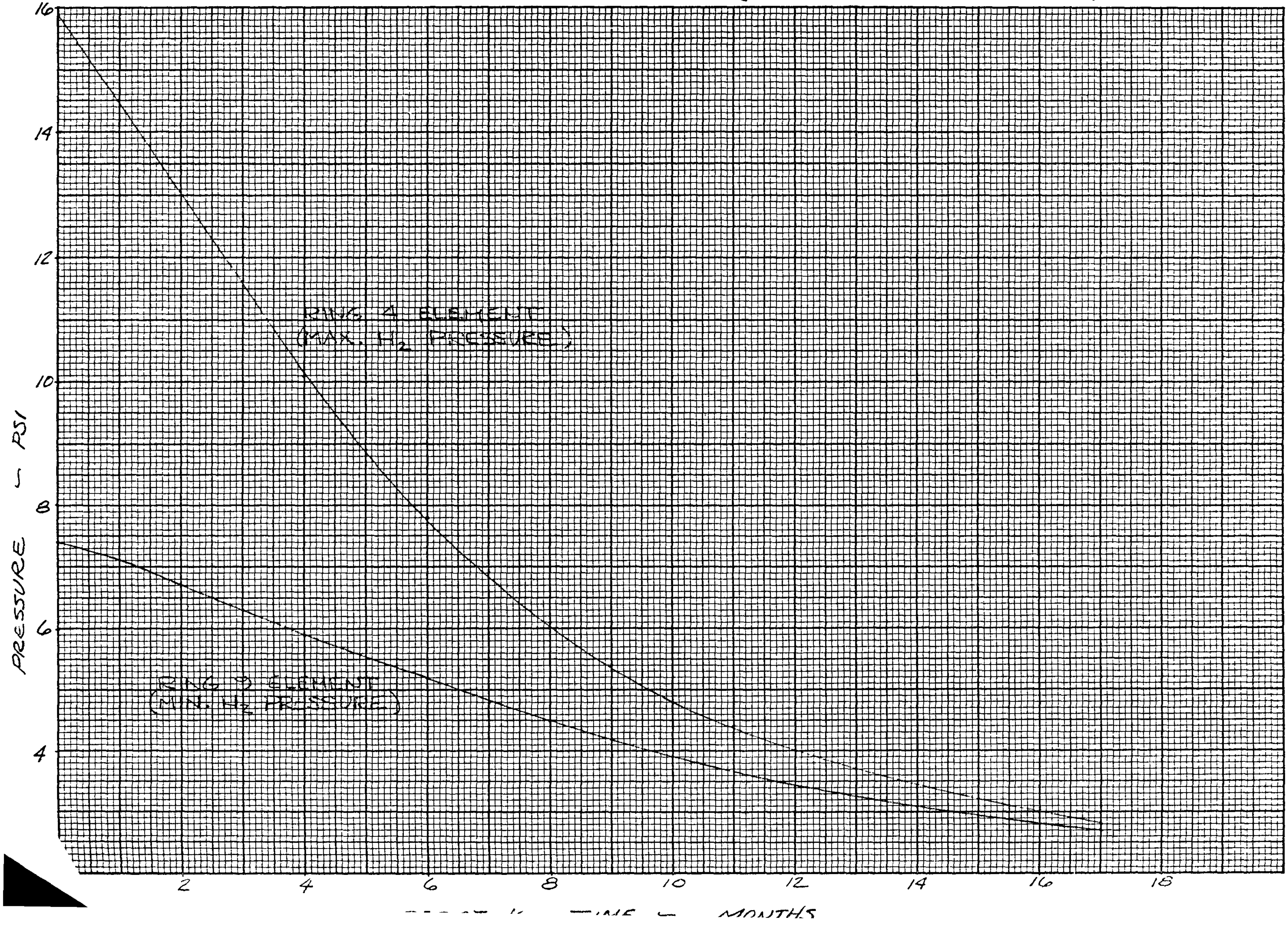

TABLE III.A.2.

Fuel Element Fission Gas Pressure
After 12,000 Hour Operation

	Fission Gas Pressure (psi)		
	Ring 1	Ring 4	Ring 9
Maximum	0.30	0.28	0.21
Nominal	0.25	0.23	0.18
Minimum	0.22	0.21	0.15

It is assumed that the fuel does not exert significant loads or strains on the cladding throughout the reactor operating lifetime. This assumption is based on fuel swelling studies and resulting S8DR axial and diametral gas gap specifications which are expected to preclude fuel-cladding contact (Ref. III.A.3.).

The preceding constitute all of the significant static operating conditions as identified by the core thermal, hydraulic, and nuclear analyses.

B. Static Thermal Conditions

The steady-state temperature and heat flux distributions in the SNAP-8 fuel element are summarized in NAA-SR-MEMO-12384 (Ref. III.B.1.) and NAA-SR-12564 (Ref. III.B.2.). For the purpose of the analysis of static stresses, only the most severe conditions were considered. These are as itemized in Table III.B.1. and defined in Figures III.B.1. through III.B.6.

TABLE III.B.1.

Static Thermal Conditions Considered in Analysis

Case No.	Description	Location Z/L	Location Ring No.	Time of Occurrence	Location of Case Definition
III-1	Maximum Circumferential Temperature Variation ("6Θ")	0.5	1	BOL	III.B.1.
III-2	Maximum "6Θ" Variation at Point of Minimum Cladding Creep Strength	0.95	7	BOL	III.B.2.
III-3	Average Radial Gradient	Avg.	Avg.	BOL	III.B.3.
III-4	Maximum Radial Thermal Gradient	0.5	1	BOL	III.B.4.
III-5	Maximum Axial Thermal Gradient Change d^2T/dL^2	0.9	4	BOL	III.B.5.
III-6	Maximum Axial Gradient at Upper End Cap	1.0	7	ALL	III.B.6
III-7	Maximum Axial Gradient at Lower End Cap	0.0	ALL	ALL	III.B.7
III-8	Maximum ΔT From Stress -Free Condition	ALL	ALL	Prior to Start-up & at EOL	III.B.8.

1. Circumferential Temperature Variation

At any axial station, the temperature distribution for constant r is given by

$$T = T_o + \left(\frac{\Delta T}{2} \right) \cos 6\theta$$

The amplitude (ΔT) of the variation as a function of axial position along the central fuel element is shown in Figure III.B.1. The two curves shown in the figure represent the nominal and zero spacing conditions for the element at beginning of life. As indicated, ΔT is a maximum at the reactor mid-plane. The variations shown are the maximum for the reactor core since ΔT decreases with increasing ring number and with operating time. Although the curves represent a symmetrical fuel assembly, little change is brought about in the ΔT values by asymmetry.

2. The minimum cladding creep strength occurs at the point of maximum cladding temperature. The value of the average cladding outer surface temperature is obtained from Figure III.B.3. At Z/L = 0.95, the temperature is 1342°F. The maximum circumferential variation is obtained by applying a radial power factor to the value obtained from Figure III.B.1.

$$T_{6\theta} = 33^{\circ}F \quad \text{at} \quad Z/L = 0.95$$

$$\text{Radial Power Factor} = \frac{0.993}{1.330} = 0.745 \quad \text{(Ref. III.B.1, Page 42)}$$

$$T_{6\theta} = (33)\,(0.745) = 24.6^{\circ}F$$

3. The average radial gradient is determined as follows:

$$\Delta_R = \text{radial temperature gradient}$$

$$\Delta_R = 1/3 \left(T_B - \overline{T}_C + \frac{\Delta_R}{2} \right)$$

FIG. III.B.1.
MAXIMUM CIRCUMFERENTIAL CLADDING TEMP. VARIATION AMPLITUDE (CENTRAL ELEMENT)

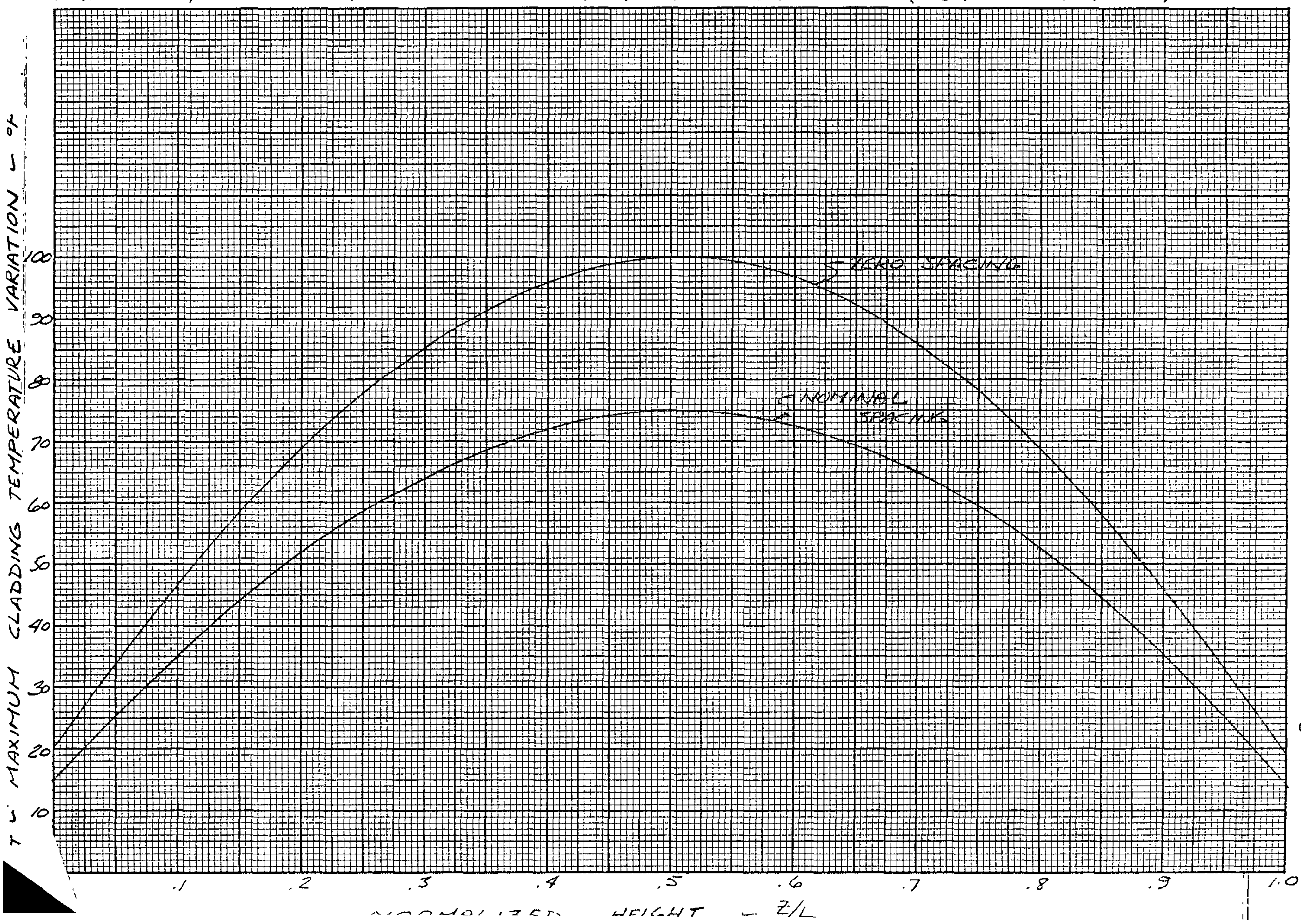

where

T_B = Barrier temperature at inner surface

$\overline{T}_C$ = Average cladding temperature from the above

Δ_R = $2/5\ (T_B - \overline{T}_C)$

Using values from Reference III.B.1, Page 19:

$$\Delta_R = 2/5\ (T_B - \overline{T}_C) = 2/5 \times 30 = 12^{\circ}F \text{ at } \theta = \pi/6$$

$$\Delta_R = 2/5 \times 18 = 7.2^{\circ}F \text{ at } \theta = 0$$

$$\Delta_{R\ avg} = 1/2\ (12 + 7.2) = 9.6^{\circ}F$$

4. For zero spacing, the circumferential gradient is increased to 100°F from 75°F (Figure III.B.1.). Applying this factor to Δ_R:

$$\Delta_{R\ avg} = 9.6 \times 100/75 = 12.8^{\circ}F \text{ for zero spacing.}$$

For the asymmetric case,

$$\Delta_{R\ max} = 2/5\ (T_B - \overline{T}_C) = 2/5 \times 48 = 19.2^{\circ}F \text{ (Ref. III.B.1, Pg. 30)}$$

Applying the factor for zero spacing

$$\Delta_{R\ max} = 19.2 \times 100/75 = 25.6^{\circ}F \text{ (zero spacing, asymmetric)}$$

5. The maximum axial thermal gradient change is produced in the upper end of the Ring 4 elements. This is shown in Figure III.B.2.

6. The maximum axial gradient in the region of the upper end caps is in the Ring 7 elements, and is approximately constant throughout reactor operation as shown in Figures III.B.3. and III.B.5.

7. The axial gradient in the lower end cap region is approximately constant for all elements, and throughout reactor lifetime. The typical gradient is shown in Figure III.B.2.

8. Maximum ΔT

The maximum isothermal temperature differential from the stress-free state being at 1400°F, the ΔT is thus 1330°F.

The stress-free condition is established during 1400°F hydrogen permeation testing. Complete stress-relaxation of barrier and metal stresses is expected to occur during this operation. Subsequent rapid cooling to lower temperatures produces cladding and barrier stresses due to differential thermal contraction.

C. Transient Thermal Conditions

Thermal transients, as described in the body and appendix of Reference III.C.1., were considered for the upper and lower end caps. The transients include hot and cold coolant "slugs" during the reactor shakedown phase, loss of primary heat rejection capability, high power scram, and low flow scram during the PCS startup and endurance phases.

Sketches of the end cap designs are shown in Figure III.C.1. Representative temperature distributions (as a function of time) for the transients considered are plotted in Figures III.C.2 through III.C.6. The number designations used in the figures refer to specific locations in the end cap regions as identified in Figure III.C.1. For the stress analysis, detailed, two dimensional, temperature distributions, obtained directly from the TAP (Thermal Analyzer Computer Program) were utilized. Transient thermal stress analyses were necessary only for the end cap regions, because the cladding response time is very low and significant gradients are, therefore, not realized. The latter conclusion assumes that there are no localized hot spots on the element cladding. This assumption is consistent with the analyses of References III.C.1, III.B.1 and I.4.

Since the cold slug transient temperature distributions are "mirror images" of the hot slug cases, the cold slug results have not been included

FIG. III.B.2. FUEL ELEMENT TEMPERATURES - RING 4, BOL

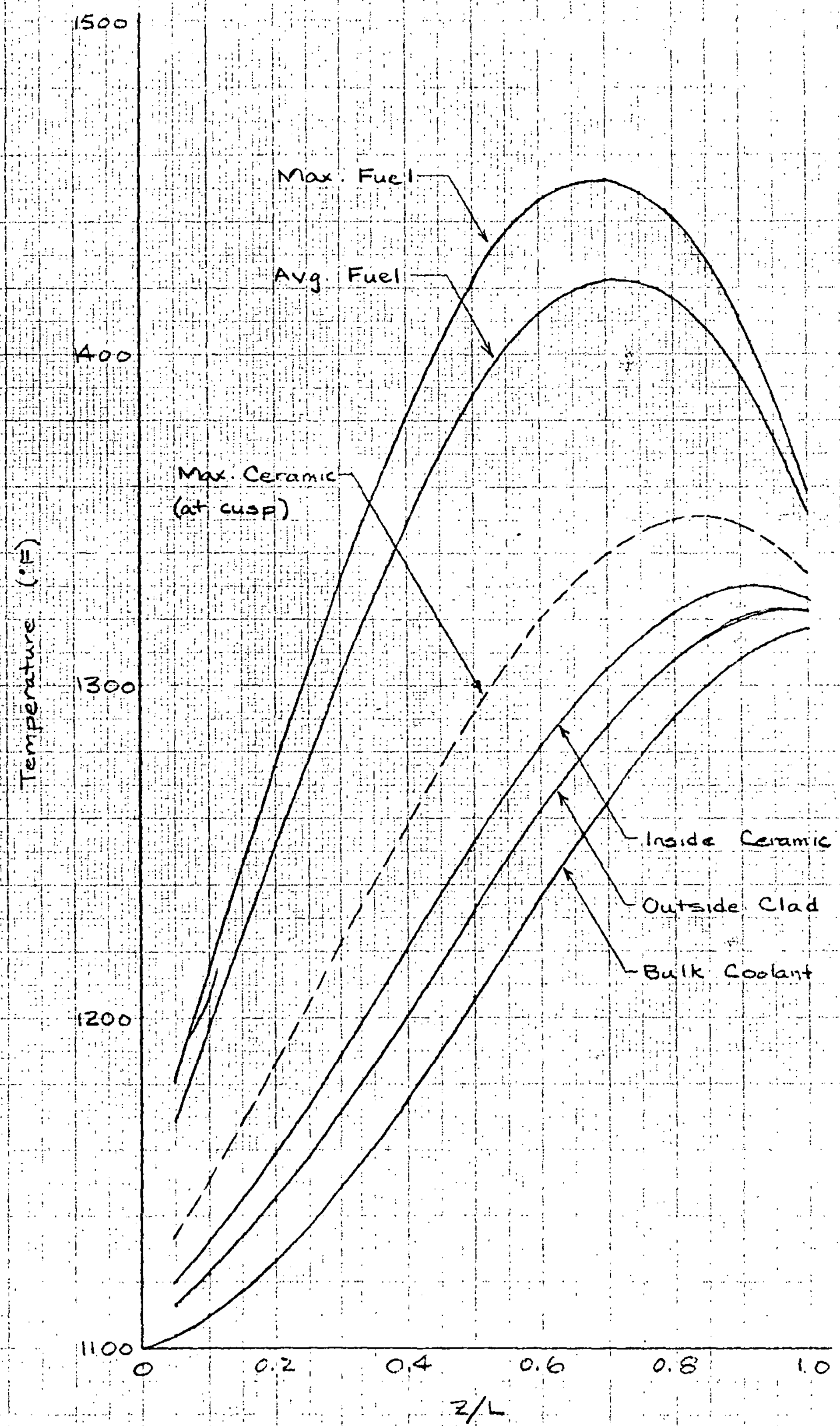

FIG. III.B.3. FUEL ELEMENT TEMPERATURES - RING 7, BOL

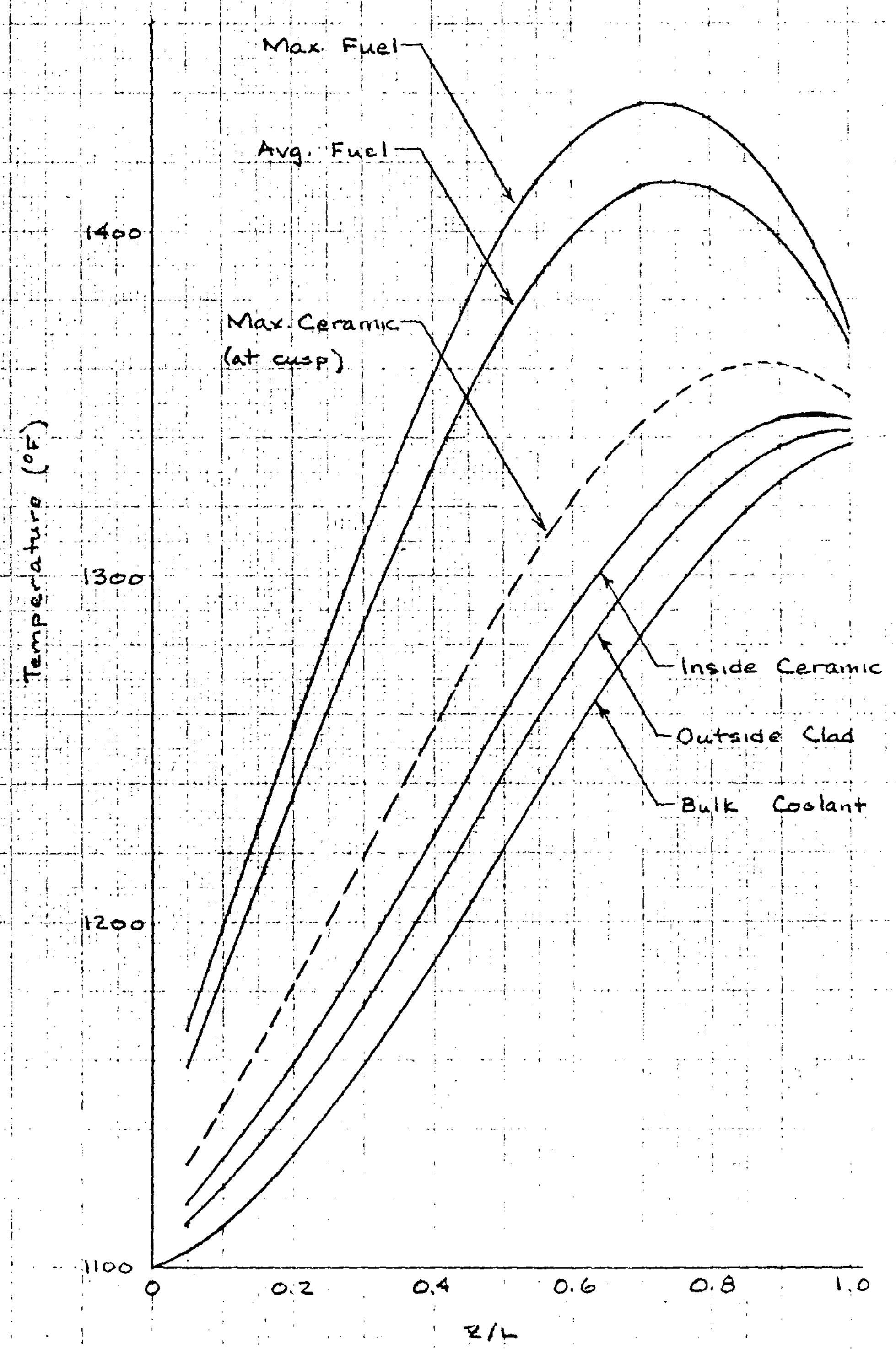

FIG. III.B.4. FUEL ELEMENT TEMPERATURES - RING 4, EOL

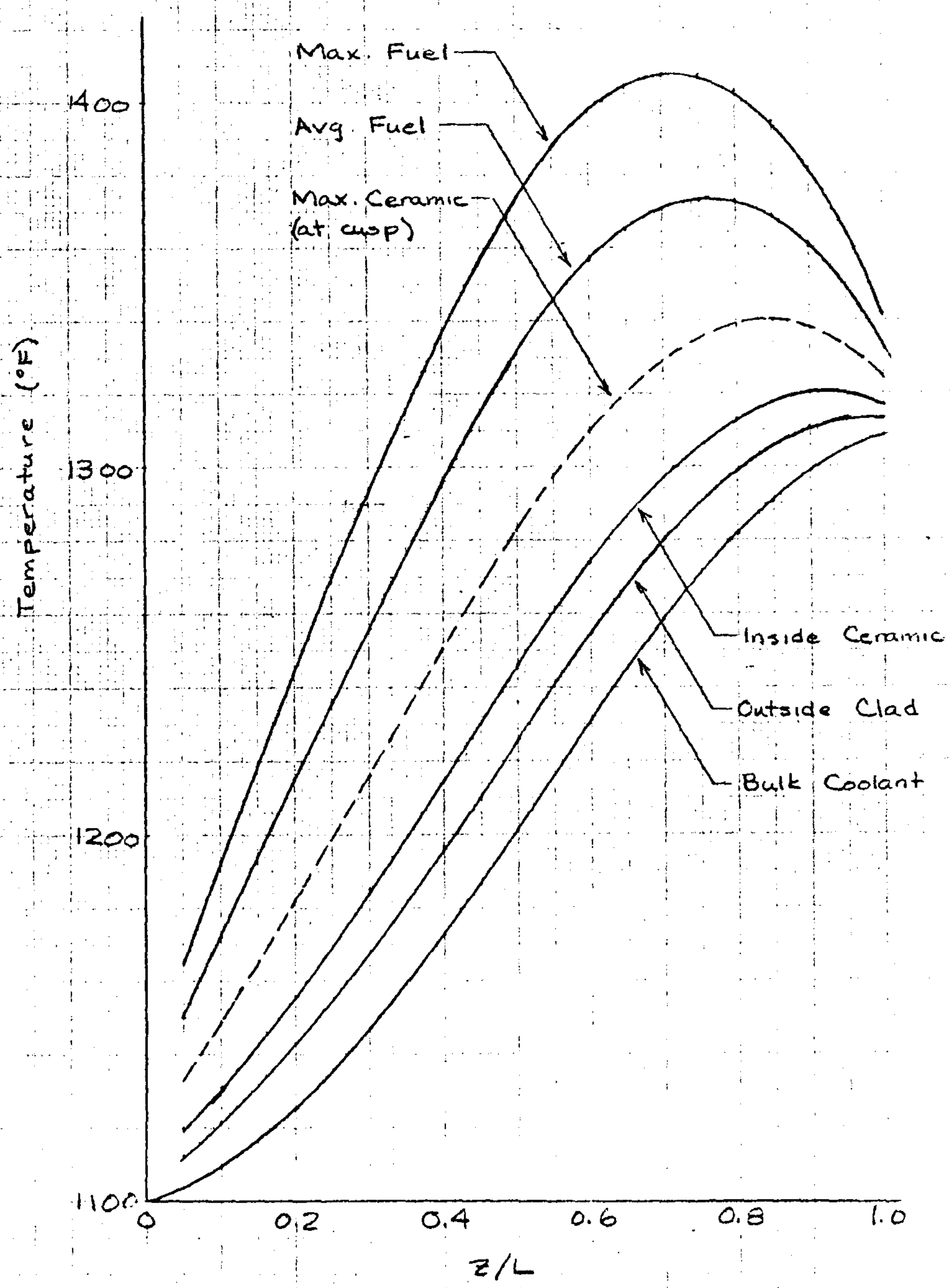

FIG. III.B.5. FUEL ELEMENT TEMPERATURES - RING 7, EOL

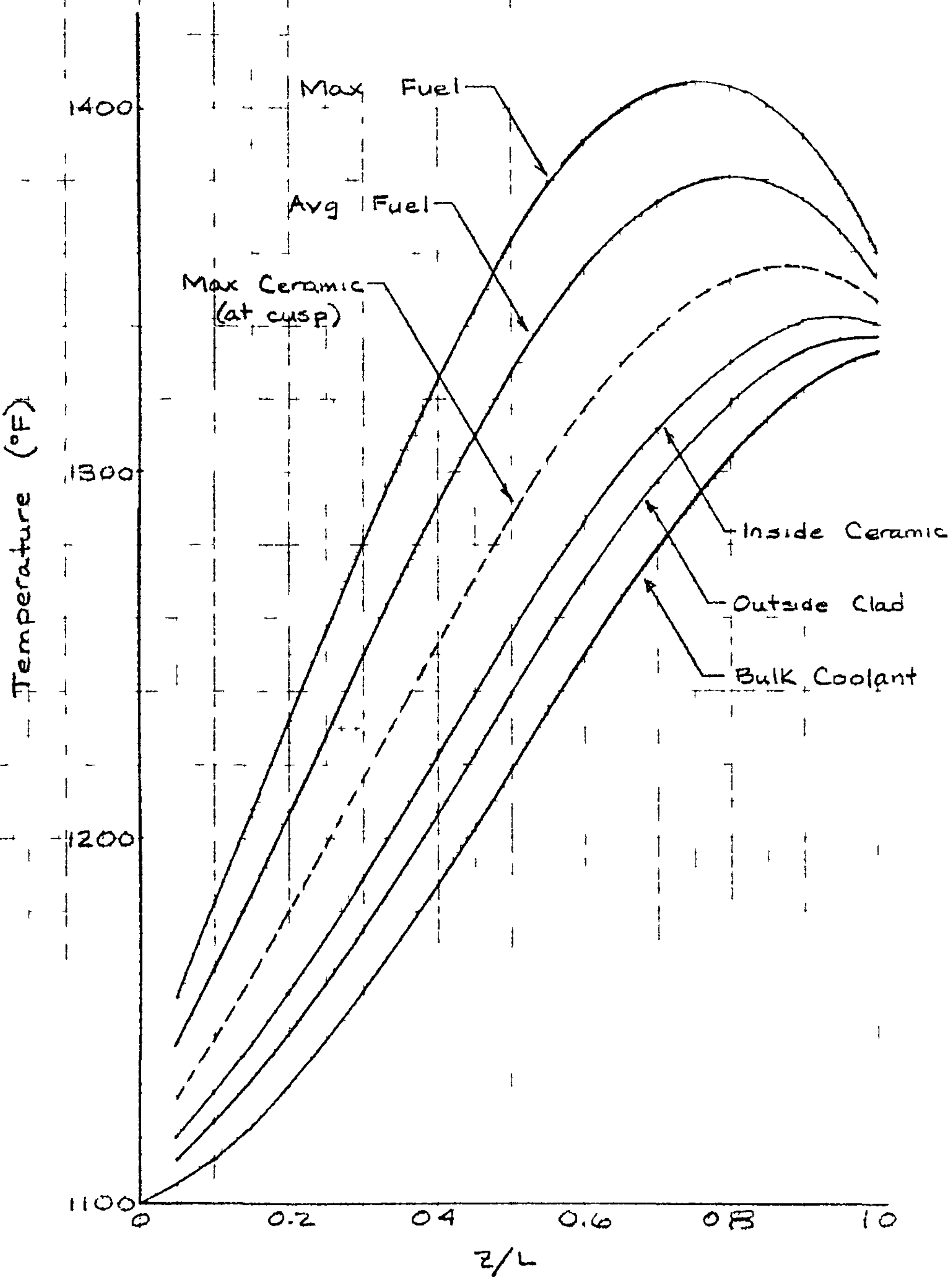

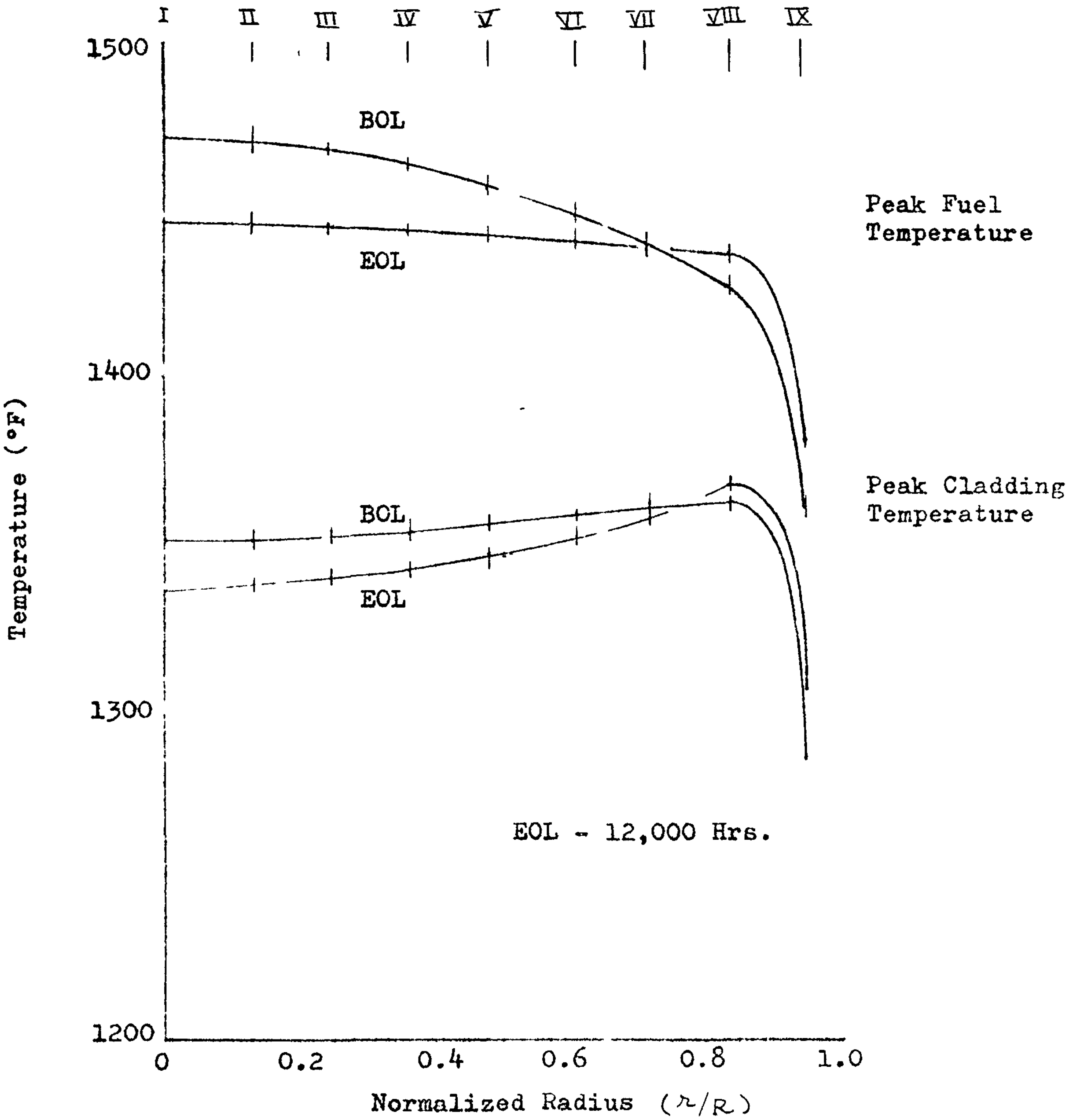

FIGURE III.B.6. S8DR Peak Fuel and Cladding Temperatures

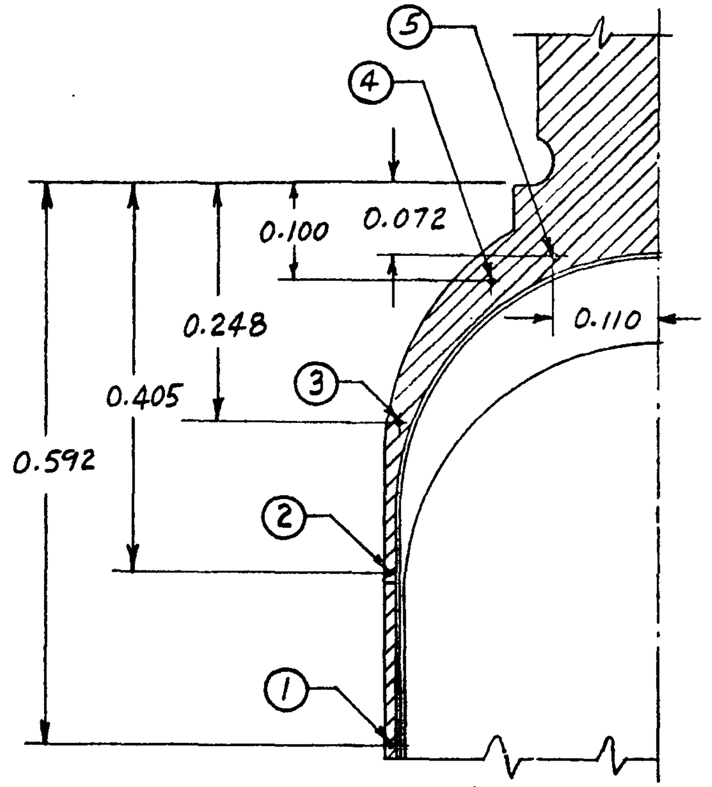

UPPER END

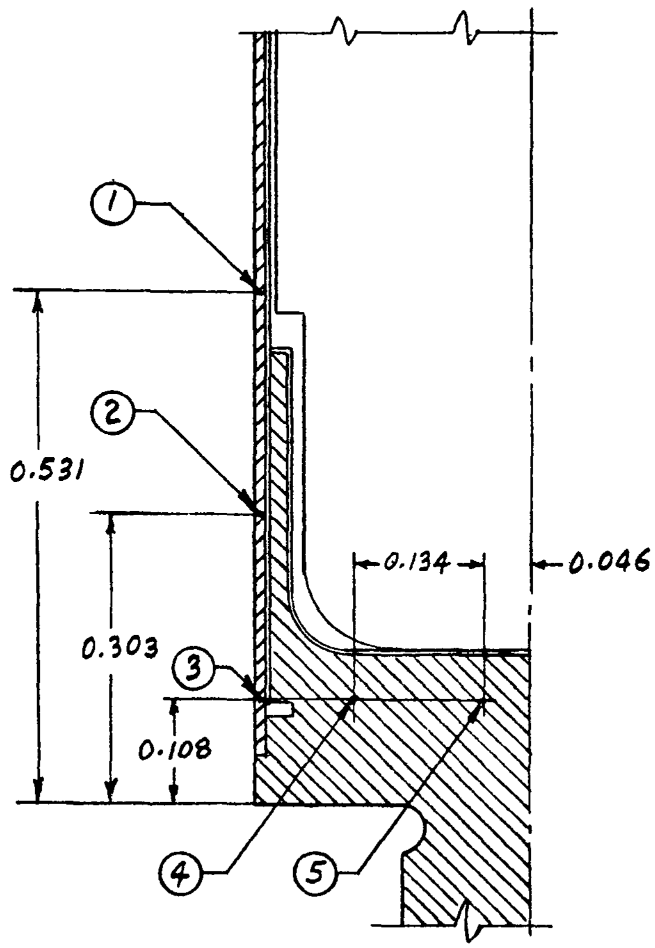

LOWER END

FIGURE III.C.1.

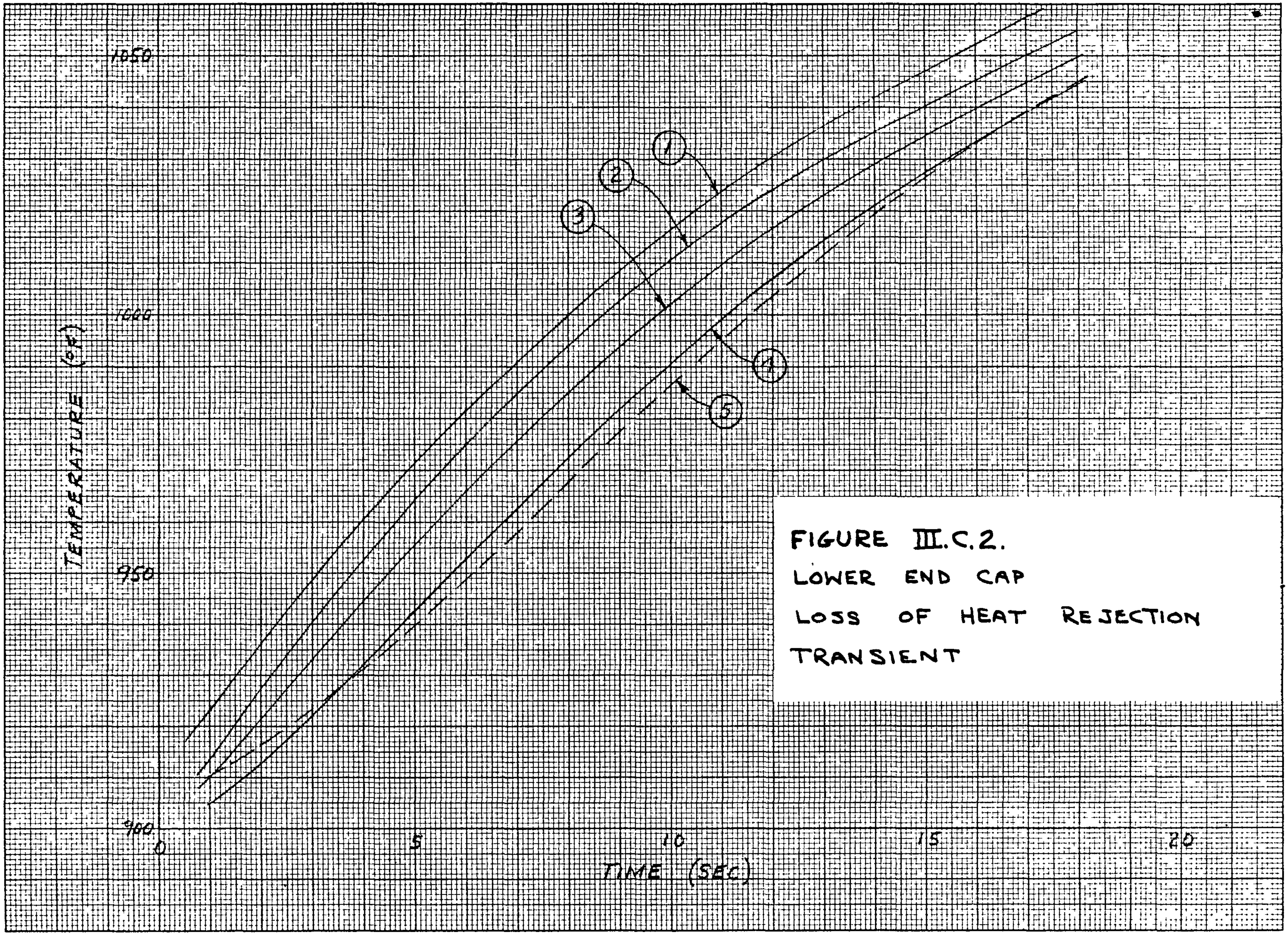

FIGURE III.C.2.
LOWER END CAP
LOSS OF HEAT REJECTION
TRANSIENT

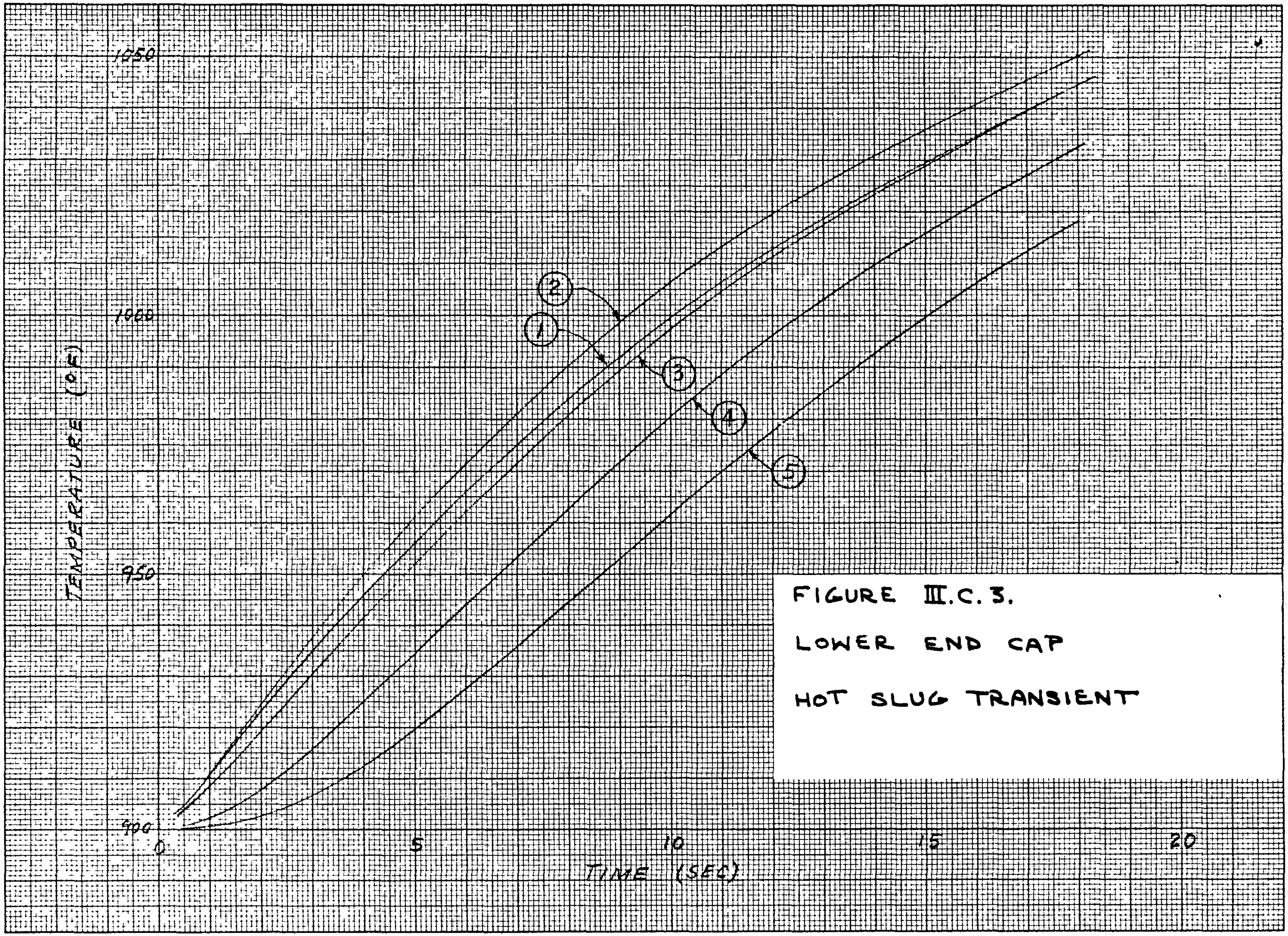

FIGURE III.C.3.
LOWER END CAP
HOT SLUG TRANSIENT

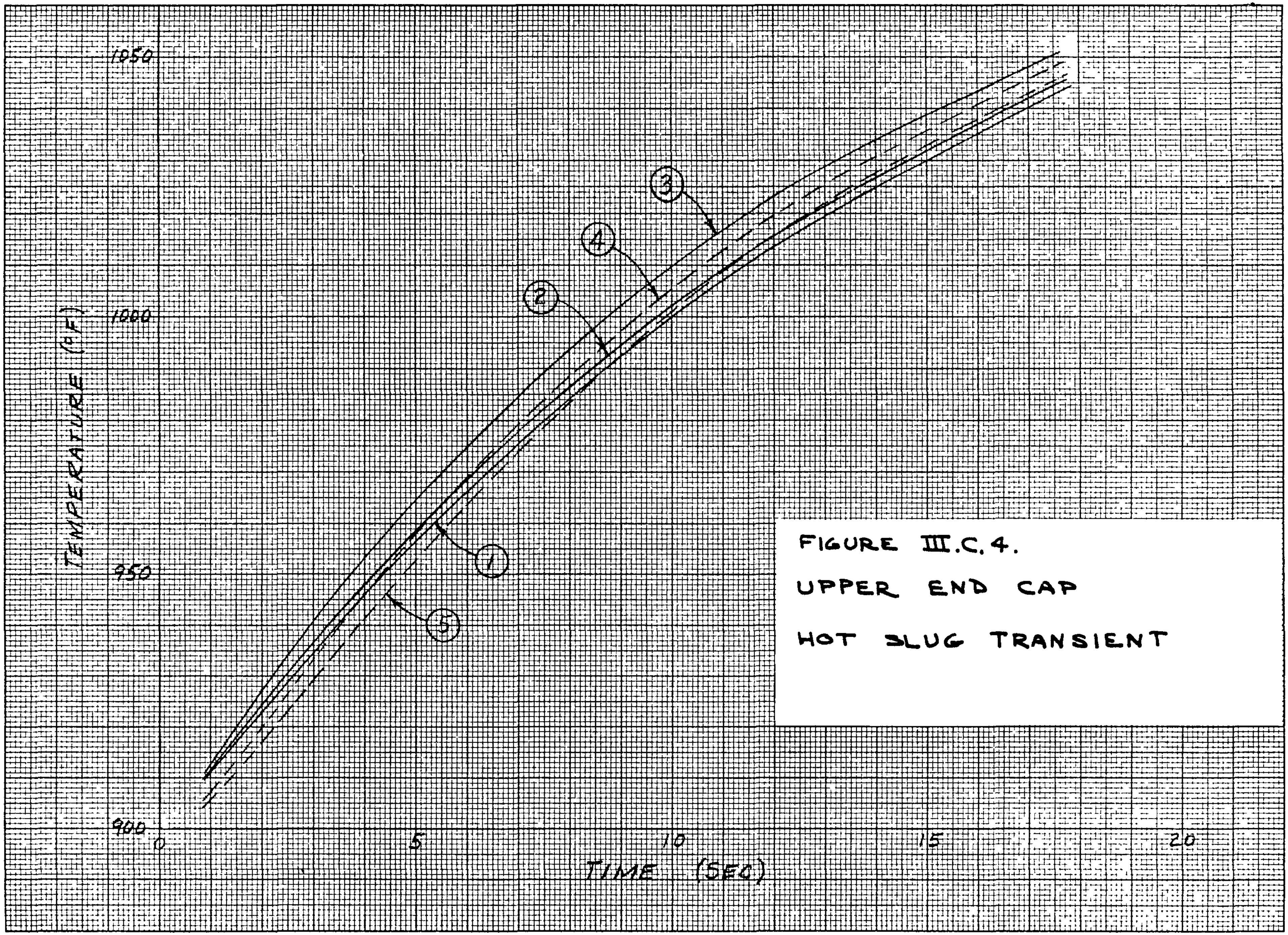

FIGURE III.C.4.
UPPER END CAP
HOT SLUG TRANSIENT

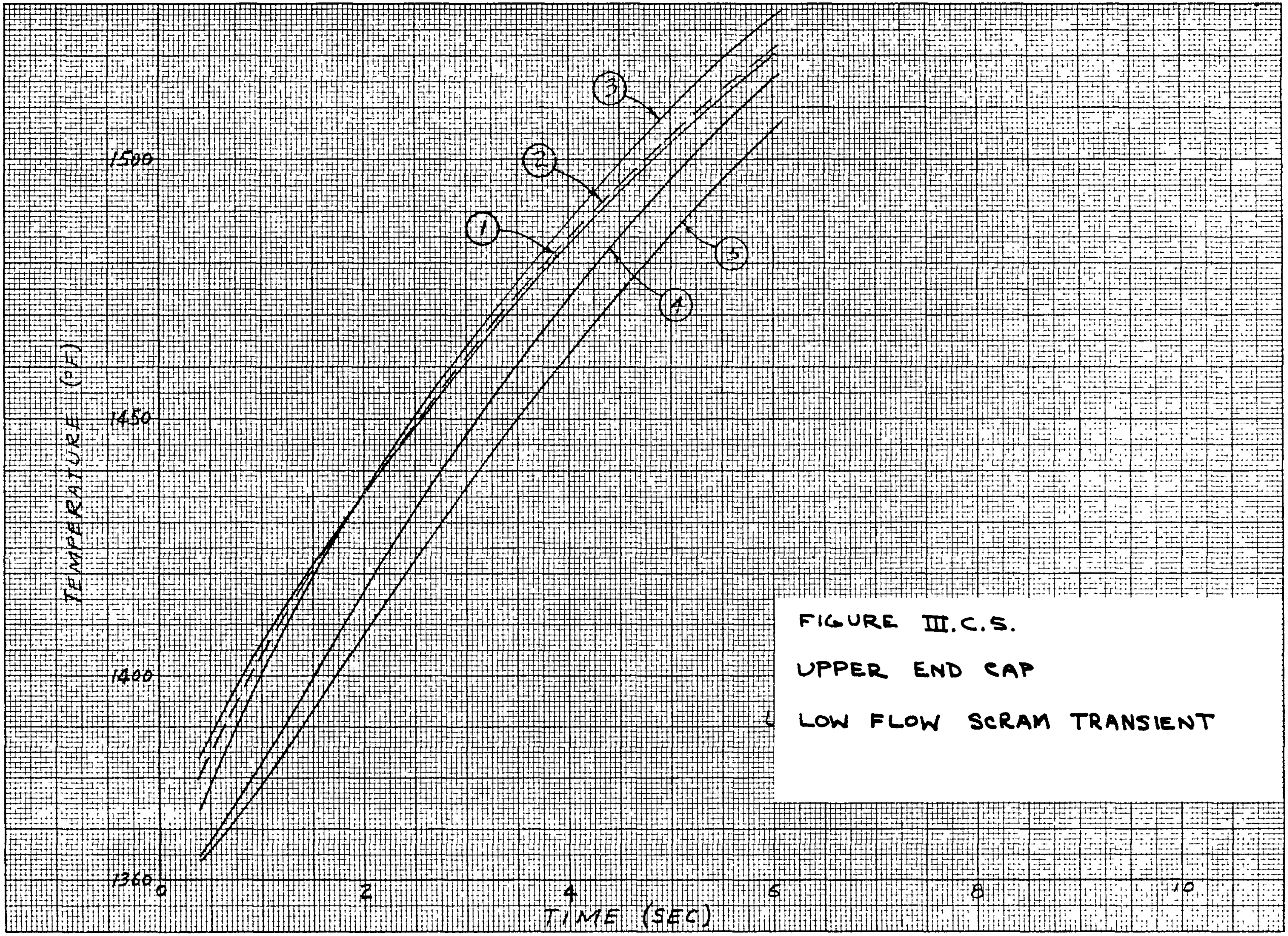

FIGURE III.C.5.

UPPER END CAP

LOW FLOW SCRAM TRANSIENT

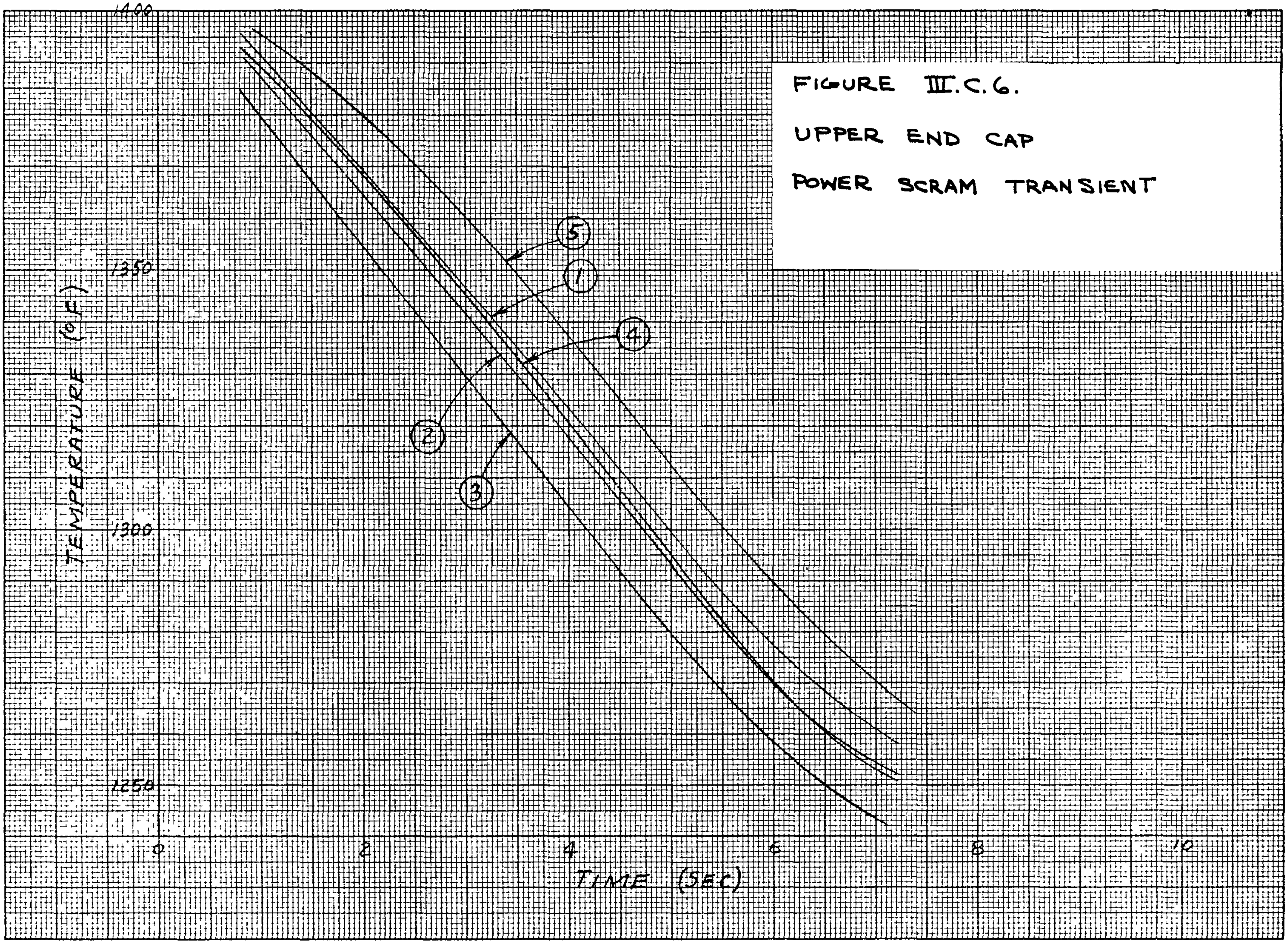

FIGURE III.C.6.
UPPER END CAP
POWER SCRAM TRANSIENT

in this section. The thermal stresses produced by cold slugs were, however, considered, and these are included in Section V.

Loss of primary heat rejection capability only affects the lower end cap region significantly. For this reason, there is no detailed temperature distribution presented for the upper end cap region for this transient. Similarly, the high power scram and the low flow scram affect only the upper end cap region, and no information is given, therefore, for the lower end cap region for these transients.

IV. MATERIAL PROPERTIES

A. Hastelloy-N

The cladding material properties used for this analysis were primarily obtained from Reference IV.A.1 and IV.A.2. The exceptions are discussed below.

To establish the allowable stress values for Hastelloy-N material, the procedure recommended in Appendix Q of Section VIII of the ASME Boiler and Pressure Vessel Code was used. During operation, the maximum credible temperature to be experienced by the fuel cladding is 1400°F. This value was used for determining the S_m allowable for the evaluation of primary and secondary stresses.

At the noted temperature, the controlling parameter is secondary creep rate limit of 1.0×10^{-7} in./in./hr. From this consideration, the value of S_m was set at 3000 psi. The creep data used were from ORNL-TM-1017.

At the time of this analysis, the fatigue properties of Hastelloy-N material had not been investigated experimentally at the temperatures of interest. Since quantitative fatigue information is necessary for calculation of service damage fractions, this was predicted based on the empirical relationships proposed by Manson and Halford (Ref. IV.A.3). The data used to generate the strain range vs cycles to failure curves are presented in Table IV.A.1 and IV.A.2.

TABLE IV.A.1

Unirradiated Hastelloy-N Tensile Data - ORNL Test Matrix: ORR S-1 Controls (0.002 in./in./min)

Heat	Specimen No.	Test Temperature (°F)	F_{TU} (psi)	RA (%)
5911	3121	1400	50,900	27.3
5911	3109	1400	47,700	14.4
5911	3115	1400	51,100	13.1
5911	2854	1400	46,700	12.5
5911	2953	1400	45,800	22.1
5911	3091	1400	47,800	13.9

TABLE IV.A.2

Irradiated Hastelloy-N - ORNL Test Matrix

Heat	Specimen No.	Test Temperature (°F)	F_{TU} (psi)	RA (%)
5911	2837	1400	32,650	3.55
5911	2839	1400	33,670	1.90

With the use of the noted data, Figures IV.A.1 and IV.A.2 were constructed. These show predicted service life for unirradiated and irradiated material. The adjusted curve plotted in each represents the estimated lower bound on lifetime reflecting the estimate of creep effects for relatively high cycle rates ($f > 0.017$ Hz). Included in the figures are the results of recent AI fatigue data of irradiated and unirradiated Hastelloy-N material reported in Reference IV.A.4. All data, to date, for 10 mil cladding, indicate that use of the adjusted curve of Figures IV.A.1 and IV.A.2 is conservative for strain cycles without long hold times at maximum stress. These reduced curves are used exclusively in Section VI to evaluate calculated cyclic stresses.

Stress relaxation curves were generated analytically for use in this effort and other SNAP 8 analyses. These curves and their derivation are given in NAA-SR-TDR-12590 (Ref. IV.A.5).

B. Ceramic Barrier

The mechanical properties of the ceramic hydrogen barrier are not well known because there has been no test program, to date, implemented to establish quantitative values for the material. Therefore, for the most part, values were assumed or estimated from typical published values for high density ceramics.

The coefficient of expansion and the modulus of elasticity of the barrier were assumed to be invariant with temperature. The values used in the analysis are given below.

$$E = 10 \times 10^6 \text{ psi}$$

$$\bar{\alpha} = \alpha_i = 3.5 \times 10^{-6} \text{ in./in.}^\circ\text{F} \quad \text{(Ref. IV.B.1)}$$

The ceramic is assumed to creep very rapidly at temperatures above 1400°F. In addition, it is assumed that displacement type stresses relax to nil in the material in less than 100 hours at temperatures above 900°F.

FIG. IV. A1.

PREDICTED STRAIN RANGE VS CYCLES TO FAILURE – NOMINAL & REDUCED VALUES
UNIRRADIATED HASTELLOY-N – 1400°F – HEAT 5911

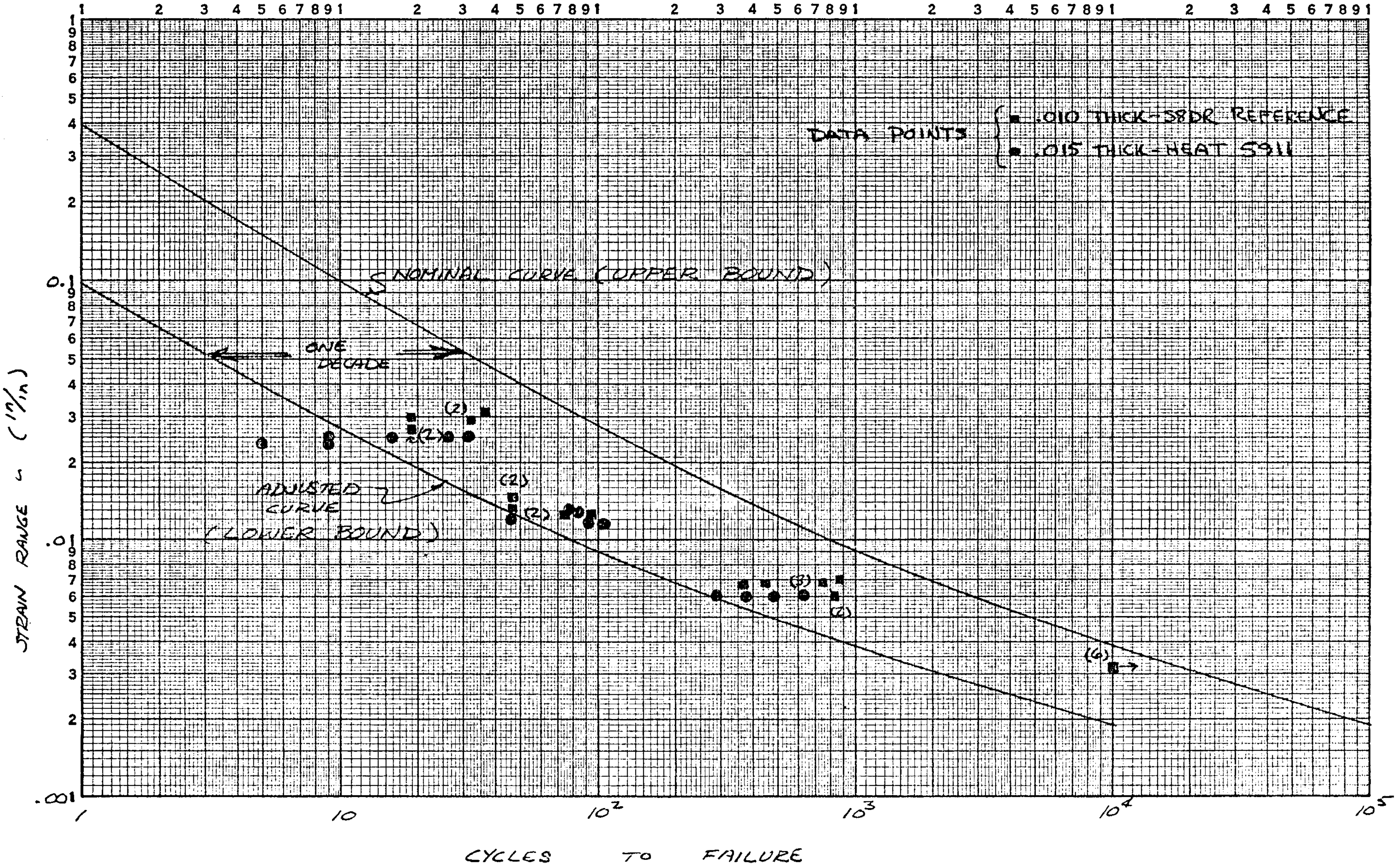

A.W.D.
6/5/67

FIG. IV. A2.

PREDICTED STRAIN RANGE VS CYCLES TO FAILURE – NOMINAL & REDUCED VALUES
IRRADIATED HASTELLOY-N – 1400°F – HEAT 5911 AW

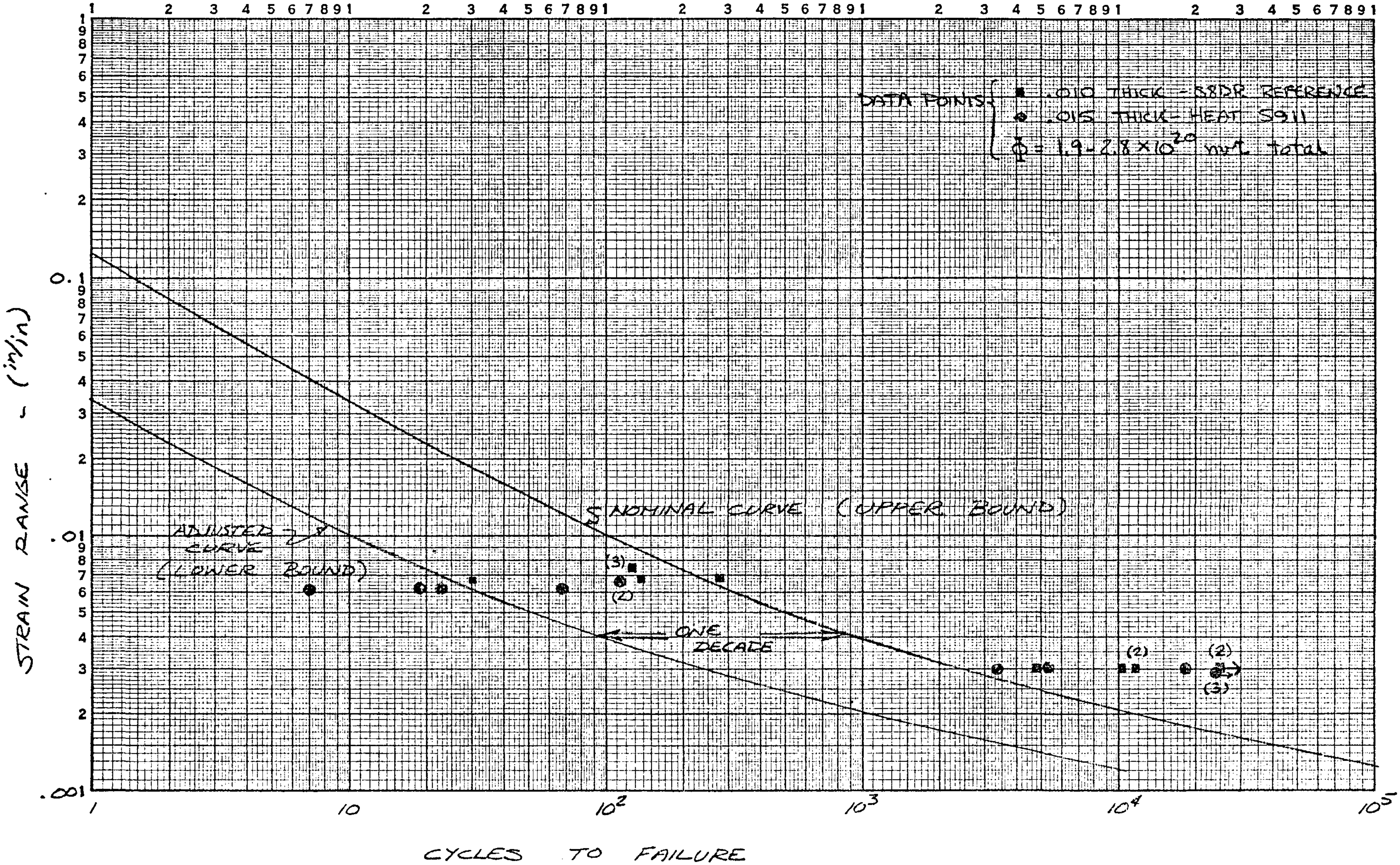

R.W.D. 6/5/67

The strength of the ceramic is assumed from typical values of Reference IV.B.2, and is as follows:

Tensile strength	$\cong$	10,000 psi
Shear strength	$\cong$	40,000 psi
Compressive strength	$\cong$	80,000 psi

V. ANALYTICAL RESULTS

A. Fabrication and Assembly Stresses

Certain processes undergone by the S8DR fuel element during fabrication and assembly produce significant stresses in the cladding and barrier materials. The discussion and summary of these stresses is given in the following section.

1. Fabrication Stresses

The fabrication steps noted below produce changes in the stress states at various locations in the fuel element.

a) Welding of the upper end cap to the cladding tube.
b) Thermal soak at 2000°F for 2 hours (Ref. V.A.1).
c) Mechanical sizing and straightening of cladding tube.
d) Thermal soak at 2100°F for 5.5 to 6.5 minutes (Ref. V.A.2).
e) Shrink-fit and welding of lower end cap to tube.
f) Thermal soak lower portion of element at 1975°F.
g) Leak testing at 1400°F for 65 hours (Ref. V.A.4).

The thermal soaks noted will all produce relaxation of the residual stresses induced by the mechanical processes. The relaxation rate is determined by use of the method outlined in Reference IV.A.4. As noted in the reference, the creep rate relationship is given by

$$\frac{d\epsilon}{dt} = 4.83 \times 10^{-4} \; \sigma^5 \exp\left(- 9.03 \times 10^4/T \right)$$

where T is in °R. From this equation, the equation relating the time required to reduce an initial stress, σ_o, to a final stress, σ_r, is determined to be

$$t = \frac{5.18 \times 10^2}{E \;\; \sigma_r^4} \exp\left(9.03 \times 10^4/T\right) \quad 1 - \left(\frac{\sigma_r}{\sigma_o} \right)^4$$

For Hastelloy-N material, the stress-strain curves above the yield point are nearly flat (zero strain hardening) (Ref. IV.A.1). Therefore, the maximum residual stress at any temperature is limited to the magnitude of the yield strength of the material. The residual stress at a temperature below that of a particular thermal process will be directly proportional to the elastic modulus assumption that the elastic strain is independent of temperature.

The calculated stress amplitudes resulting from the various operations are summarized below.

a. Stresses in Top Cap Region (Ref. V.A.5)

(1) Induced by Ceramic Coating

$\sigma_\theta = \sigma_z = +31{,}000, \quad \sigma_r = 0$ at 70°F

$\sigma_\theta = \sigma_z = +4{,}000, \quad \sigma_r = 0$ at 1300°F (operating temperature)

(2) Induced by Chrome Coating

$\sigma_\theta = \sigma_z = -1450, \quad \sigma_r = 0$ at 70°F

$\sigma_\theta = \sigma_z = +1450, \quad \sigma_r = 0$ at 1300°F

(3) Tube Sizing Residual Stresses

$\sigma_\theta = \sigma_z = +2200, \quad \sigma_r = 0$ at 70°F

$\sigma_\theta = \sigma_z = +1730, \quad \sigma_r = 0$ at 1300°F

b. Stresses Near Element Mid-Plane (Ref. V.A.5)

(1) Induced by Ceramic Coating

$\sigma_\theta = \sigma_z = +31{,}000, \quad \sigma_r = 0$ at 70°F

$\sigma_\theta = \sigma_z = +6{,}000, \quad \sigma_r = 0$ at 1200°F (operating temperature)

(2) Induced by Chrome Coating

$\sigma_\theta = \sigma_z = -1450, \quad \sigma_r = 0$ at 70°F

$\sigma_\theta = \sigma_z = +1450, \quad \sigma_r = 0$ at 1200°F

(3) Due to Fuel-Cladding Interference

70°F:

$\sigma_z = +\ 4,900$ at point of load

$\sigma_z = -\ 4,900$ opposite load

$\sigma_z = 0$ at 90° to load

$\sigma_\theta = +\ 11,650$ at load, outer surface of clad

$\sigma_\theta = -\ 11,650$ at load, inner surface of clad

$\sigma_\theta = 0$ remote from load

$\sigma_r = 0$

1200°F:

$\sigma_z = +\ 1,600$ at point of load

$\sigma_z = -\ 1,600$ opposite load

$\sigma_z = 0$ at 90° to load

$\sigma_\theta = +\ 3,890$ at load, outer surface of clad

$\sigma_\theta = -\ 3,890$ at load, inner surface of clad

$\sigma_\theta = 0$ remote from load

$\sigma_r = 0$

c. Lower End Cap (Ref. V.A.5)

(1) Induced by Ceramic Coating

$\sigma_\theta = \sigma_z = +\ 31,000$ at 70°F, $\sigma_r = 0$

$\sigma_\theta = \sigma_z = +\ 8,500$ at 1100°F, $\sigma_r = 0$ (operating temperature)

(2) Induced by Chrome Coating

$\sigma_\theta = \sigma_z = -\ 1450$ at 70°F, $\sigma_r = 0$

$\sigma_\theta = \sigma_z = +\ 1450$ at 1100°F, $\sigma_r = 0$

(3) Induced by Residual Shrink-Fit Pressure

At 70°F:

Inner Surface:

$\sigma_z = 0$

$\sigma_\theta = +3100$

$\sigma_r = -110$

Outer Surface:

$\sigma_z = 0$

$\sigma_\theta = 2980$

$\sigma_r = 0$

At 1100°F:

Inner Surface:

$\sigma_z = 0$

$\sigma_\theta = +2550$

$\sigma_r = -90$

Outer Surface:

$\sigma_z = 0$

$\sigma_\theta = +2450$

$\sigma_r = 0$

2. Assembly Stresses (Ref. V.A.5)

a. Due to Element to Element Interference

$\sigma_z = -1000$ at point of load

$\sigma_z = +1000$ opposite load

$\sigma_z = 0$ at 90° to load

$\sigma_\theta = -1100$ at load, outer surface of clad

$\sigma_\theta = +1100$ at load, inner surface of clad

$\sigma_\theta = 0$ remote from load

$\sigma_r = 0$

B. Static Load Stresses

Membrane stresses in the fuel element cladding were calculated based on the static external and internal pressures reported in Section III.A. The analysis and results are presented below.

$$\sigma_\theta = -\frac{P\,r}{t} = -P\,\frac{(0.275)}{(0.010)} = -27.5\ P$$

$$\sigma_r = -P \quad \text{outer surface}$$

$$\sigma_r = 0 \quad \text{inner surface}$$

$$\sigma_z = -P\ r/2\ t = -13.8\ P$$

$$P = (\text{NaK System Pressure}) - (\text{Fuel Element Pressure})$$

From III A:

$$P = (35 - 16.2) = 18.8 \text{ psi} \quad (\text{minimum})$$

$$P = (35 - 2.8) = 32.2 \text{ psi} \quad (\text{maximum})$$

The pressure varies from the minimum value to the maximum due to the loss of hydrogen pressure as shown in Figure III.A.1. The result is a changing cladding membrane stress. The values are noted in Figure V.B.1.

At the end caps, the static pressure leads to bending stresses due to the cylinder-plate junction discontinuity. The stress values are given by:

$$\sigma_Z \max = \pm 1.55\ Pr/t = \pm 42.6\ P \ (\text{tensile on outer surface})$$

$$\sigma_\theta = 1.31\ Pr/t \quad \text{outer surface}$$

$$\sigma_\theta = 0.39\ Pr/t \quad \text{inner surface}$$

$$\sigma_r = 0$$

FIG. V.B.1. CLADDING MEMBRANE STRESSES

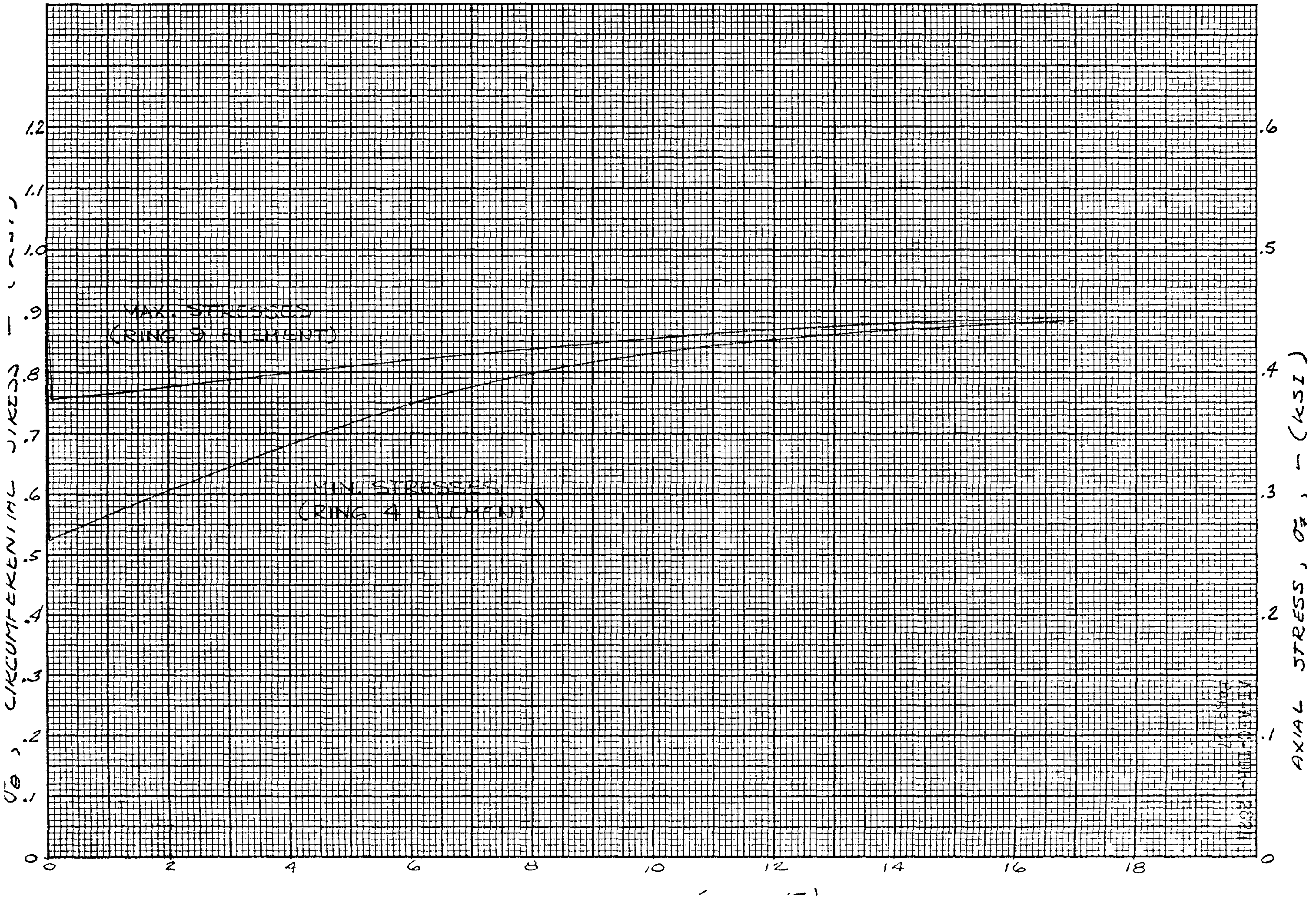

If the system is pressurized prior to power generation, the net compressive pressure will be 35 psi. Using this value, the secondary stresses are found.

$$\sigma_{z_{max}} = \pm 1490 \text{ psi} \quad \text{tensile on outer surface}$$

$$\sigma_{\theta} = + 1260 \text{ psi} \quad \text{outer surface}$$

$$\sigma_{\theta} = + 380 \text{ psi} \quad \text{inner surface}$$

$$\sigma_{r} = 0$$

The average fuel temperatures required to rupture the fuel element cladding, based on ultimate Hastelloy-N tubing strength, were determined by P. M. Magee as reported in Reference V.B.1. In this study, the average H/Zr of the fuel varied from 1.72 to 1.77. Since the hydrogen dissociation pressure increases with temperature, the failure temperature was considered to be that which produced the hydrogen pressure which would, in turn, produce the cladding failure stress. The reported results show that the minimum temperature required is 1635°F.

The fuel element was analyzed to determine the maximum allowable external pressure on the cladding (corresponding to a NaK system surge pressure). The calculations (presented below) indicate that elastic buckling will occur when the net compressive pressure is 82 psi. It was assumed, for this evaluation, that the duration of the high-pressure condition is short.

MAXIMUM OPERATING TEMPERATURE = 1340°F

$E = 24.6 \times 10^6$ psi

$\nu = 0.3$

$F_{cy} = 25000$ psi

USING THE PROCEDURE FROM NAA S&ID STRUCTURES MANUAL, SECTION 9.30

+2 -1 +1 +2

$$Z = \frac{L^2}{rt}\sqrt{1-\nu^2} = \frac{(17)^2(.955)}{(.280)(.010)} = 9.86 \times 10^4$$

$$K_p = 0.6(Z)^{.544} = 0.6\,(9.86 \times 10^4)^{.544} = 312.5$$

THE BUCKLING PRESSURE IS:

$$p = K_p \frac{\pi^2 E}{12(1-\nu^2)} \frac{t^3}{L^2 r}$$

$$p = \frac{(312.5)(\pi^2)(24.6 \times 10^6)(1 \times 10^{-6})}{(12)(.955)(17^2)(.280)} = \frac{75870}{927}$$

$p = 81.8$ psi ← ELASTIC BUCKLING

C. Static Thermal Stresses

1. Radial Thermal Gradients

The occurrence of a radial thermal gradient in a cylindrical shell leads to stresses at the outer and inner surfaces according to the expression

$$\sigma_z = \sigma_\theta = \pm \frac{E\,\alpha\,(T_i - T_o)}{2\,(1 - \nu)}$$

$$\sigma_r = 0$$

at points remote from end effects (Reference V.C.1). The upper sign refers to the outer surface, indicating that a tensile stress will act on this surface if $T_i > T_o$.

Under steady-state conditions, the radial thermal gradients become negligible in the end cap regions. Use of the above equation is therefore justified since the noted qualification is satisfied.

The significant gradient conditions are defined by Cases III-3 and III-4 in Table III.B.1. The resultant stresses for these cases are as follows.

Average Radial Gradient

$$\sigma = \pm \frac{(250)(9.6)}{(1.4)} = \pm 1720 \text{ psi}$$

Maximum Radial Gradient (Center element; Z/L = 0.5)

$$\sigma = \pm \frac{(250)(25.6)}{(1.4)} = \pm 4560 \text{ psi}$$

2. Circumferential Thermal Gradients

Cladding stresses due to circumferential temperature variations were studied by Hsieh (Reference V.C.2) and found to follow the relationship

$$\sigma_Z = -1/2\, E\, \alpha\, (\Delta T) \cos 6\,\theta$$

$$\sigma_r = \sigma_\theta = 0 \qquad \text{for elastic conditions.}$$

Using the ΔT values noted in Section III.B. the stresses are:

Maximum "6θ" variation (center element, Z/L = 0.5)

$$\sigma_Z = \pm \left(\frac{250}{2}\right) (100) (1) = \pm 12{,}500 \text{ psi}$$

Maximum "6θ" variation at point of minimum cladding creep strength (Ring 7, Z/L = 0.95)

$$\sigma_Z = \pm \left(\frac{250}{2}\right) (25) (1) = \pm 3130 \text{ psi}$$

These stresses are tensile (+) in the regions where cos 6θ is negative ("cold" strips).

At the top end cap, the "6θ" stress becomes

$$\sigma_Z = \pm \frac{250}{2} (19) (1) = \pm 2380 \text{ psi}$$

Due to the presence of the circumferential temperature variation, and the associated stresses, strain concentrations are produced at the hot line zones where neighboring fuel tubes come in closest proximity. This occurs, at operating temperatures, because hot region creep rates are significantly higher than those of the adjacent cold zones.

The magnitude of hot line creep strains and stresses were determined with the use of the digital computer code CREEP (Ref. V.C.3). Figure V.C.1 shows the maximum axial (z) stresses and maximum creep strains resulting from the circumferential temperature variation plotted against time. The calculations are representative of the Case III.1, of Section III (center element, midplane, zero spacing, 1250°F average cladding temperature). The curves are terminated at 1200 hours; the design lifetime for the S8DR reactor. Figure V.C.2 is an extension (inverted) of the hot strip maximum axial plastic strain curve of the previous figure. Here, a straight line

FIG. V.C.1.

68 STRESS & AXIAL PLASTIC STRAIN vs TIME

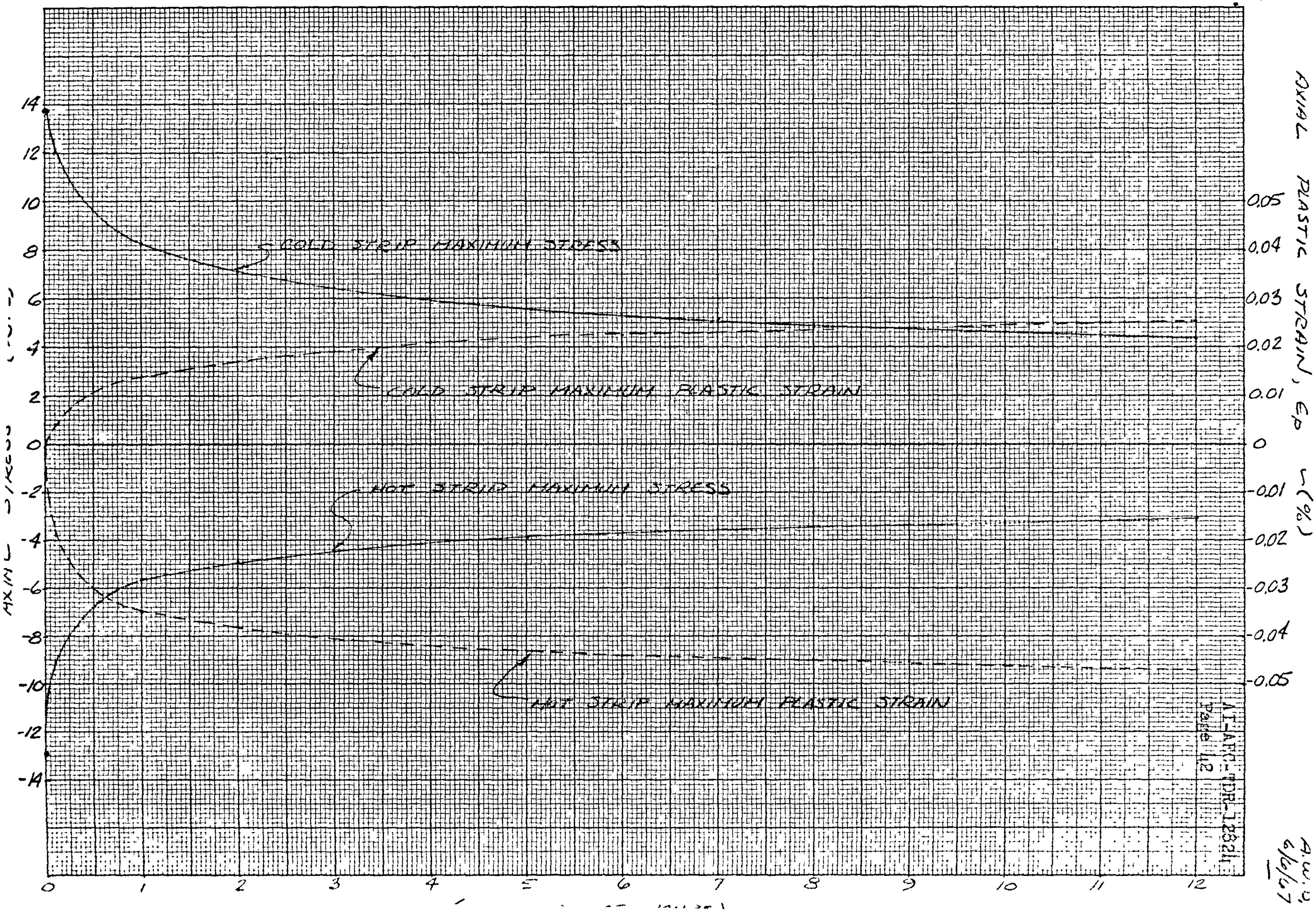

A.W.C.
6/6/67

FIG. V.C.2.

PLASTIC STRAIN DUE TO 6θ STRESS VS TIME – HOT STRIP

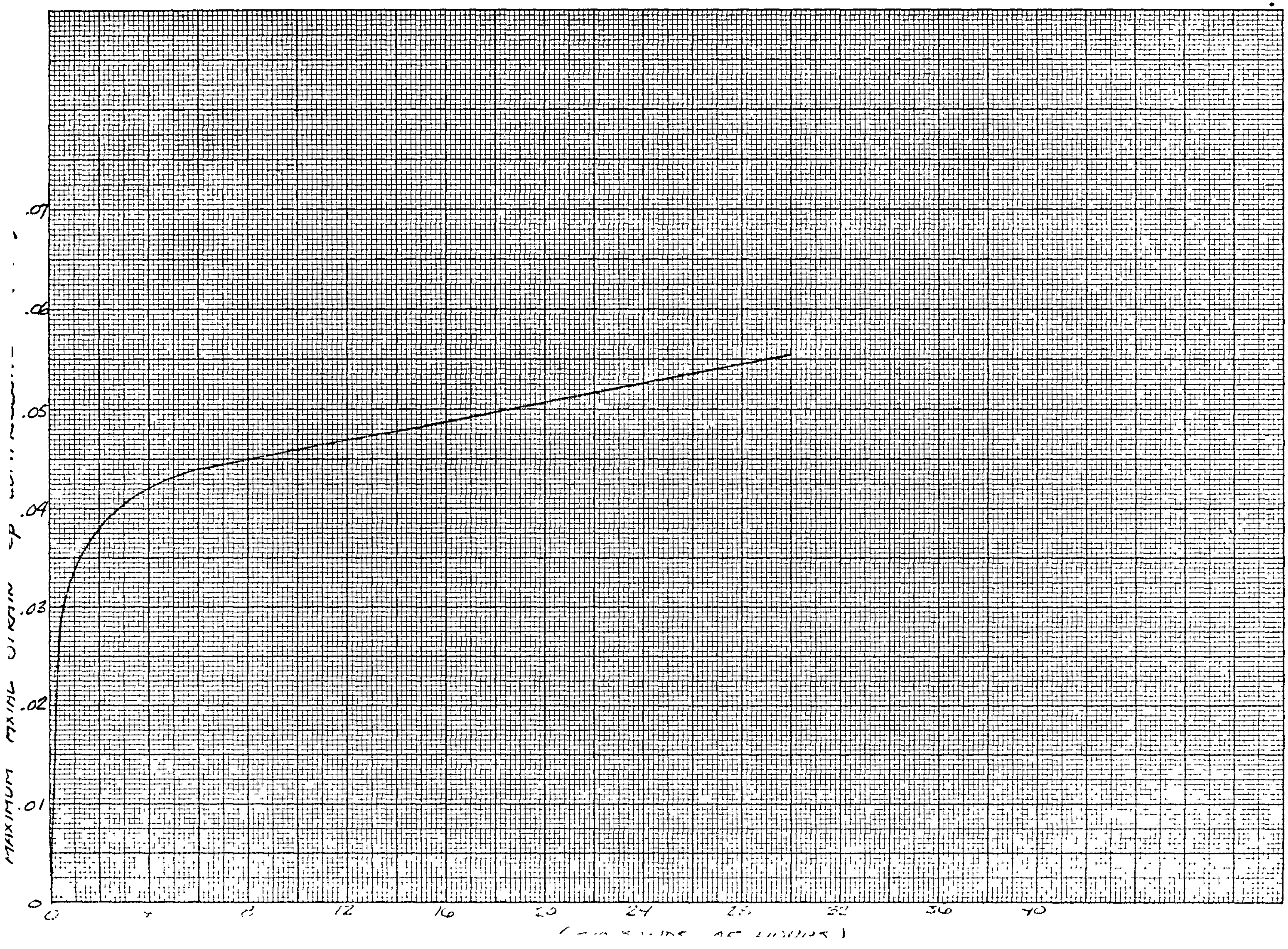

extrapolation was made to 30,000 hours to examine conditions at that point in time.

The condition defined as Case III-2 of Section III (maximum 6θ variation at the point of minimum cladding creep strength) has been analyzed for creep-collapse in Section V.D.

3. Axial Thermal Gradients

The maximum axial thermal gradient occurs in the lower end cap region as defined in Section III.B., and is equal to 16.5°F/inch. Using this value, and assuming that the cladding is built-in to a rigid end cap, the stresses are:

$$\sigma_Z = 0.706 \; E \, \alpha \sqrt{rt} \quad (\Delta T)$$

$$\sigma_Z = (0.706)\,(250)\,(0.053)\,(16.5) = 154 \text{ psi}$$

This result indicates that the maximum axial gradient produces a very small maximum stress. Therefore, the stresses produced by axial gradients will be assumed to be negligible throughout the element cladding.

4. Isothermal Conditions

The maximum ΔT from the stress-free condition (Case III-8 of Section III.B) has been included in Section V.E., and evaluated as a transient condition rather than static.

D. Creep Collapse

Due to the combined actions of net compressive pressure and initial tubing ovality, the fuel cladding is subject to creep collapse at high operating temperatures. This problem has been studied extensively by Y. Pan (Ref. V.D.1.) who developed a method for calculating creep deflections and predicting creep buckling of a thin-walled cylinder under uniform external pressure and arbitrary temperature gradients. The method allows for shell materials with arbitrary creep characteristics, and thus may include the effects of primary creep as well as secondary, if desired. The analytical model forms the basis for the digital computer code, CREEP (Ref. V.C.4) which numerically solves the differential equations by a finite difference technique and time-wise iterations.

From numerous cases studied, it was found that the minimum creep-collapse time occurs at the fuel cladding location of maximum creep rate. This location is the same as that defined by Case III-2, Section III; i.e., Z/L = 0.95, Ring 7. At this position, the average temperature is 1342°F with a 25°F circumferential variation (Section III.B.2.). A more severe thermal condition was analyzed with the use of CREEP for two values of external pressure; 43 and 28 psi. The actual temperatures input were 1350°F average, 50°F 6θ ripple, and 5°F radial gradient. The initial cladding ovality assumed for these cases was 0.002 inch (semimajor axis minus semiminor axis). The results of this evaluation are shown in Figure V.D.1. and V.D.2. The curves indicate that collapse occurs at approximately 370,000 hours with 43 psi NaK pressure, and at approximately 2,200,000 hours with 28 psi. As noted in Section III.A, the maximum long term net compressive pressure is 32 psi. Interpolation between the previously calculated values shows that collapse would occur at approximately 1,300,000 hours for the latter pressure.

Figure V.D.3. has been constructed using the above results for the average-time-to-collapse curve. The curve in the figure noted as minimum time to collapse was plotted by applying a factor of 1/5 to the higher curve. The latter factor is intended to provide for potential creep rate scatter (Ref. V.D.2.).

The analytical results presented do not take the fuel dimensions into account. That is, the cladding is analytically allowed to strain progressively until collapse would theoretically occur for a hollow tube. In actuality, the fuel will be present to restrict excessive diametral cladding strains. With fuel swelling, fuel restraint will occur long before collapse would occur. The analysis is, therefore, considered to be conservative.

FIGURE V.D.1.
PLASTIC STRAIN VS TIME - CREEP COLLAPSE - P = 43 PSI, 25/5/1810 (FROM R.D. ELLIOTT, RUN 41, CASE 2)

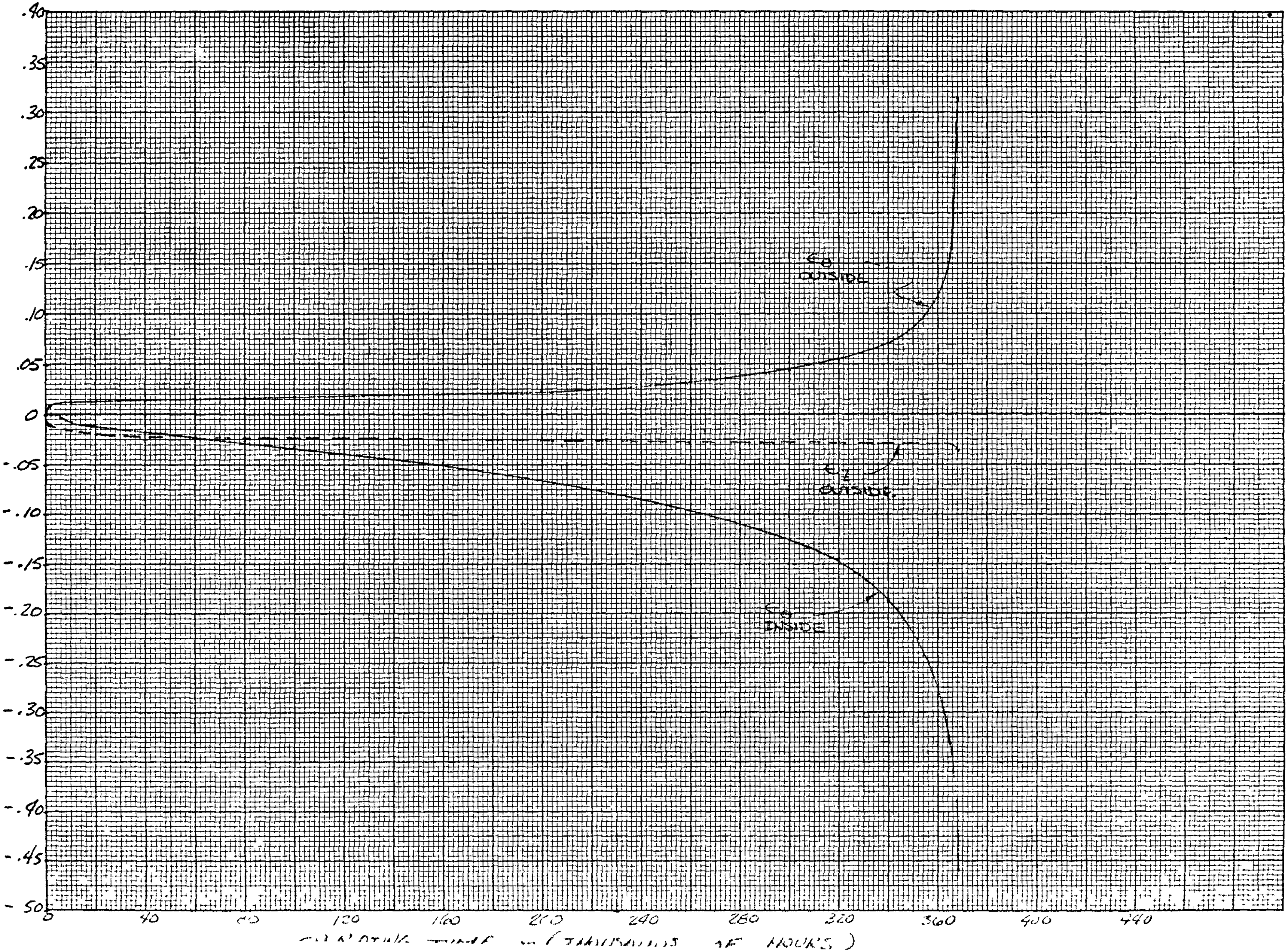

FIG. V.Q2.
PLASTIC STRAIN vs TIME - CREEP COLLAPSE P = 28 PSI TEMP - 25/5/1810 (FROM R.D. ELLIOTT'S RUN 44, CASE 1)

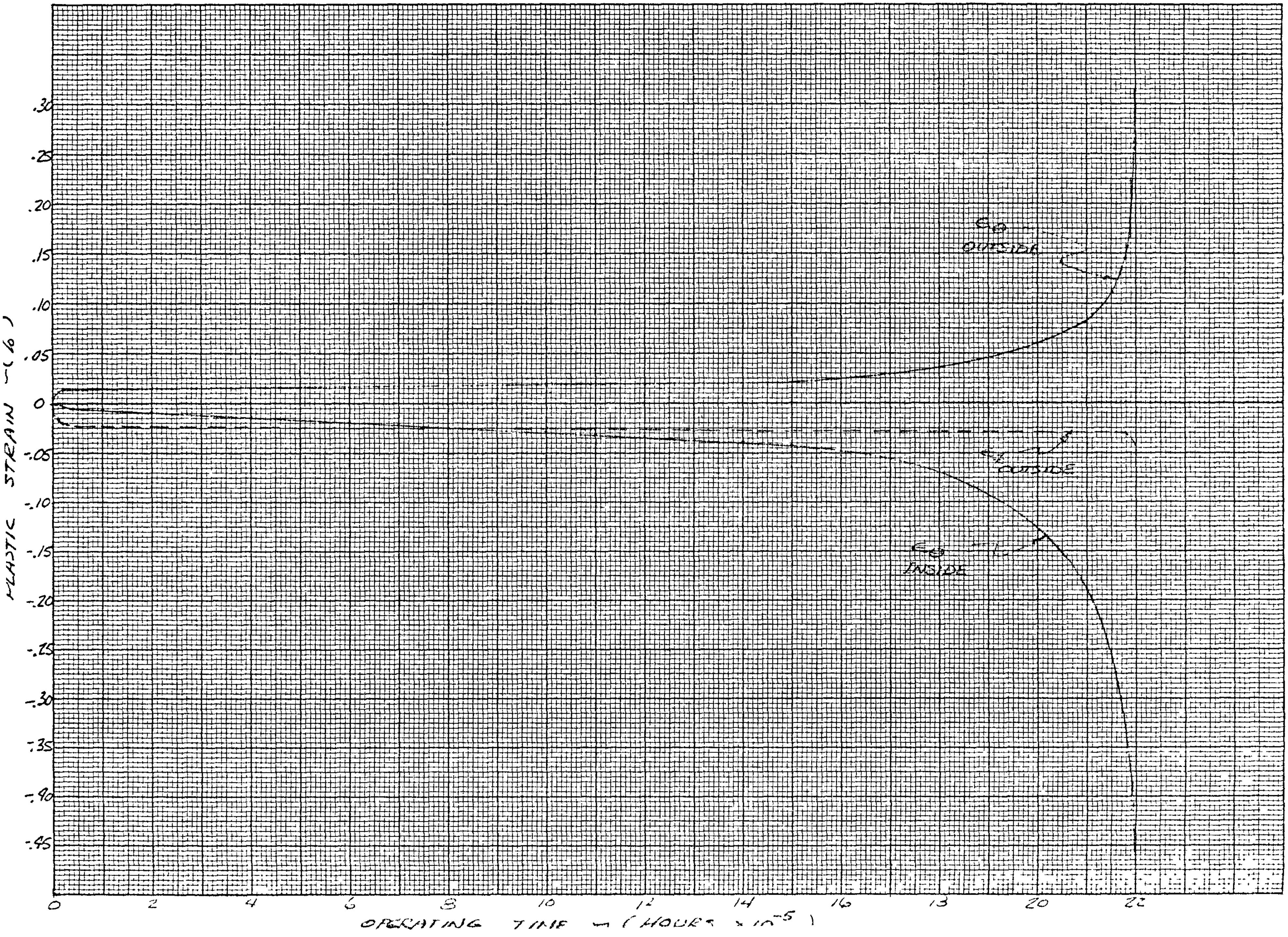

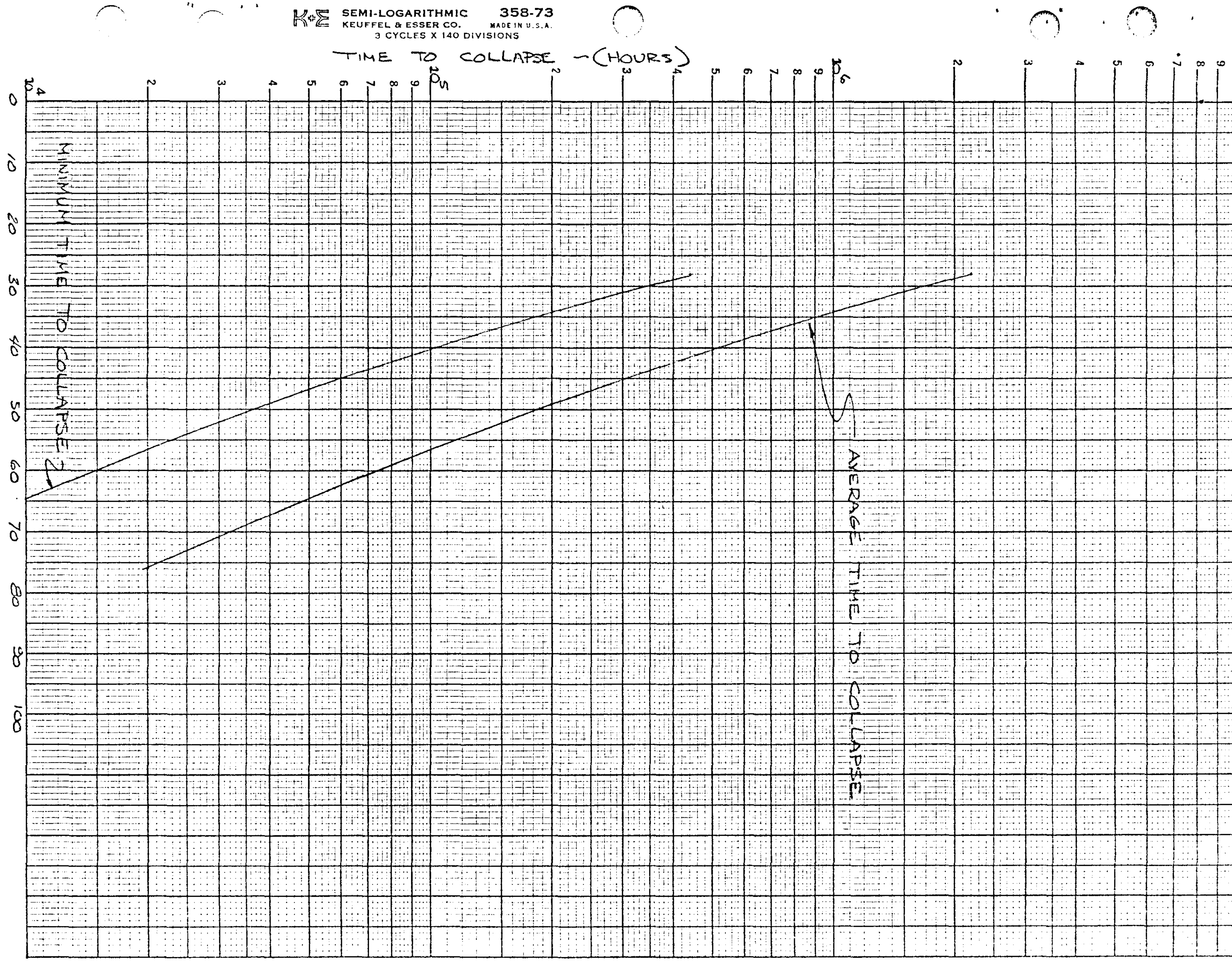

FIG. V.D.3. TIME TO CREEP COLLAPSE VS. NET NAK PRESSURE

E. Transient Thermal Stress Analysis - General Discussion

The fuel element assembly is "thermal-soaked" isothermally at 1400°F for approximately 40 hours during permeation testing. Since the ceramic barrier (Reference V.E.1) creeps readily at this temperature, it has been assumed that all residual stresses in the assembly are relieved during the operation. The stress-free condition is therefore 1400°F, and all thermal stress calculations are based accordingly.

The glass is assumed to creep readily at temperatures above 900°F. Although values have not been measured, experience and recent investigation (Reference V.E.1) indicates that the glass creep rate is considerably greater than that of Hastelloy-N at these temperatures. Below 900°F, the creep-rate of the glass is assumed to be nil. The effect of the accelerated creep at temperatures in the operating range, is to reduce the stresses due to differential thermal expansion of the metal and glass. Therefore, the high initial thermal stresses induced in the cladding by the barrier are reduced with time at static operation. These considerations were incorporated into the fuel element stress analysis evaluation.

The stress analysis was accomplished with the use of the modified AVCO shell analysis digital computer code (Reference V.E.2). The code solves plane stress problems for thin shells of revolution by a finite difference solution of the differential equations of elastic equilibrium. The analytical model used is shown in Figures V.E.1 and V.E.2. Neither end cap lends itself readily to division into simple geometric shapes required for input to the code. Therefore, the model used is an approximation of the actual structure, and the computer output should be evaluated accordingly. The models yielded accurate results as judged by the satisfaction of boundary conditions and the absence of strain inconsistencies in the interior portion of the regions.

Transient thermal stresses were analyzed with temperature inputs as described in Section III.C. The analytical approach used treated the problem as quasi-steady-state. That is, the temperature distributions at each interval of time during the transient period were examined, and the

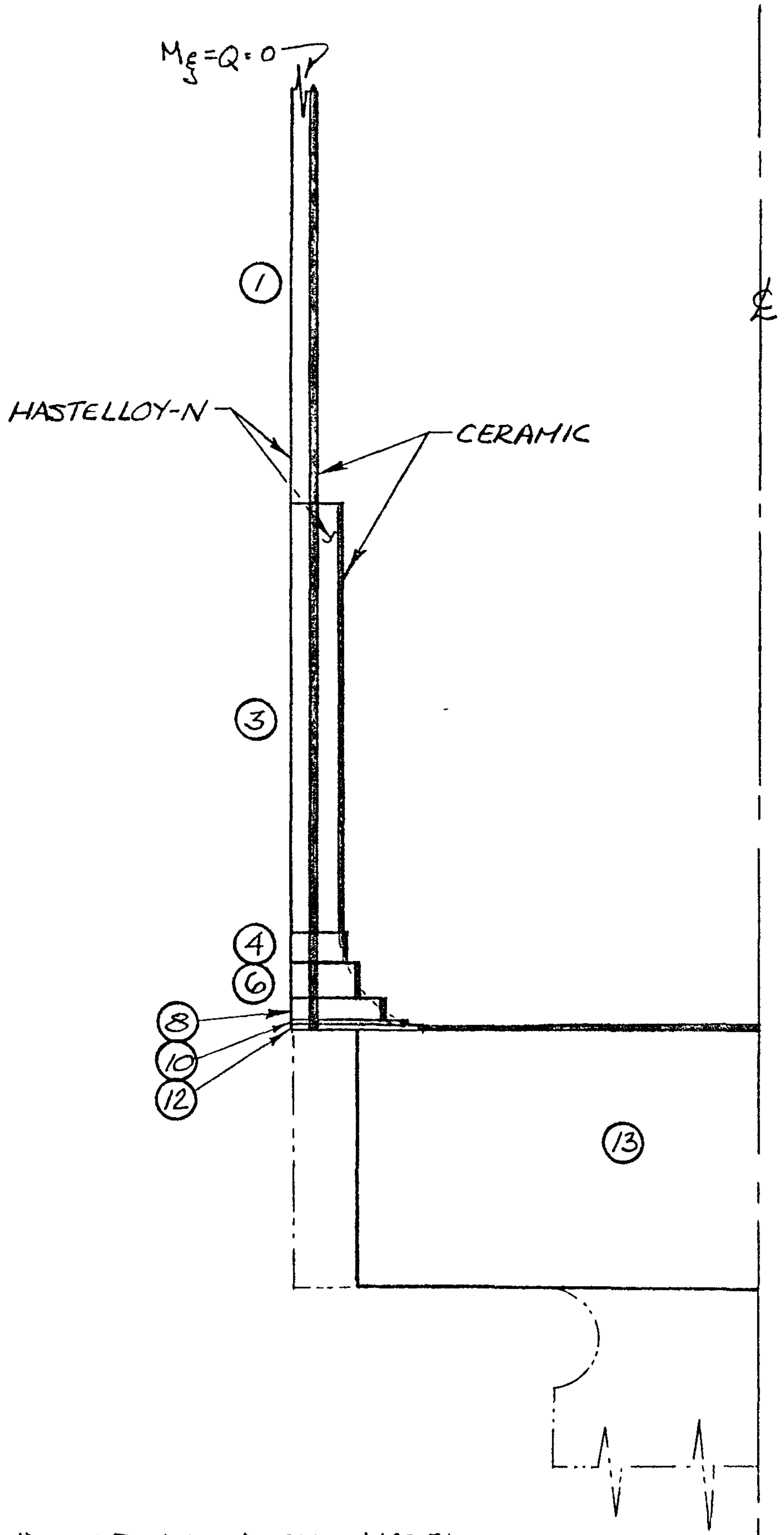

FIG V.E.1.

LOWER END CAP ANALYTICAL MODEL

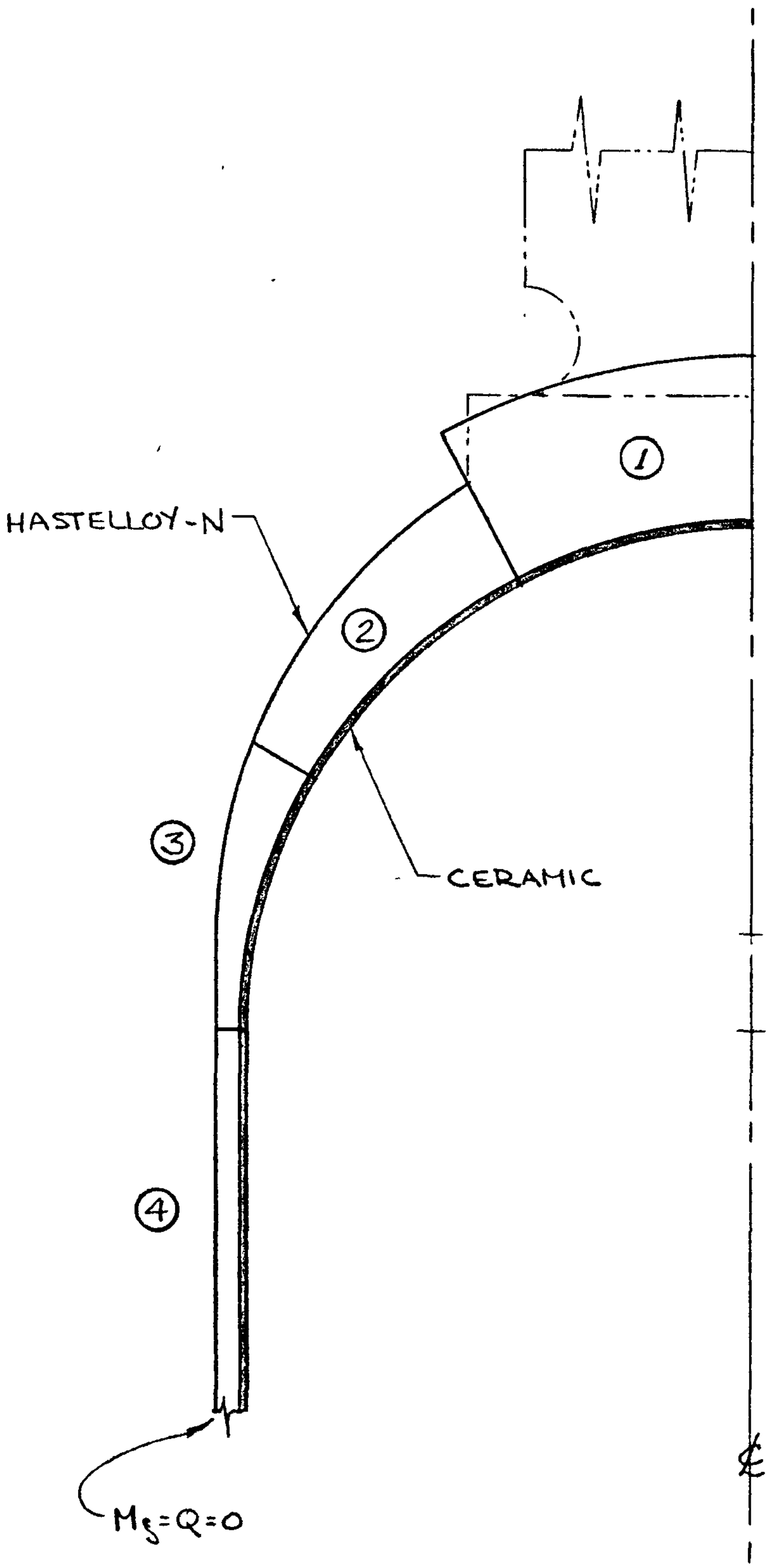

FIG. V.E.2.
UPPER END CAP ANALYTICAL MODEL

instantaneous distribution was then used as input for the analysis of the shell stresses as though the condition were a static one. The resultant stresses represented the range (alternating stress amplitude) realized during the transient.

1. Lower End Cap

Table V.E.1.1. summarizes the maximum and minimum stresses for each of the significant lower end cap thermal transients. The temperature distributions for the transient conditions exist exclusively during the transient period. The transient stresses, therefore, are not additive to any other thermal stresses.

Stress distribution plots are presented in Figures V.E.1.1., V.E.1.2., and V.E.1.3. The solid curves represent the circumferential stresses for the outside surface of the cladding, and the dashed curves represent the meridional stresses for the internal surface of the cup. The six other principal metal stresses have not been plotted since they do not include the maximum and minimum calculated values for the transients. The thick-walled end cap stresses (Region 13) have also not been included in the figures because they are not of principal interest. The barrier (ceramic) stresses vary only slightly over the end cap region for any thermal condition. Because of this, these stresses were also excluded from the figures.

The 200°F hot slug transient is the mirror image of the 200°F cold slug. Figure V.E.1.1., then, may be used to represent the latter transient by reversing the signs of the stresses. Figure V.E.1.3 may also be used to represent the room temperature isothermal condition by suitable modification of the ordinate scale (apply factor of - 6.1).

The curves show the effects of the structural discontinuity at the upper end of the cup (junction of Regions 3 and 1). Portions of the curve have been smoothed to eliminate fictitious stress discontinuities produced by the analytical model discontinuities. The model discontinuities were necessitated by the computer code's inability to properly handle sharply tapered regions.* The tapered portion of the end cap was,

*Recent modifications to the code (Ref. V.E.3) have eliminated this shortcoming.

therefore, approximated by a series of short, concentric cylindrical steps as shown in Figure V.A.1.

TABLE V.E.1.1

Lower End Cap Maximum and Minimum Transient Thermal Stresses

Operating Condition	Maximum and Minimum Stresses (psi)	
	Cladding	Barrier
Isothermal @ Room Temp.	(+25,600) (3) +24,300 (4) + 3,570 (12)	- 85,100 (4) - 92,700 (8)
$200^{\circ}F$ Hot Slug Transient	+ 950 (6) - 3,850 (6)	+ 6,620 (6) 0 @ t = 0
$200^{\circ}F$ Cold Slug Transient	+ 3,850 (6) - 950 (6)	0 @ t = 0 - 6,620 (6)
Loss of Heat Reject Transient	+ 800 (8) - 3,850 (12)	+ 6,510 (6) 0 @ t = 0
+ $200^{\circ}F$ Isothermal	- 600 (12) - 4,000 (4) (- 4,200) (3)	+ 15,360 (8) + 14,000 (4)

Numbers in circles ◯ denote region number for stress location (see Figure V.A.1.)

VE METAL STRESSES – 58DS LWR END CAP – REF. DESIGN – 200F HOT SLUG TRANSIENT

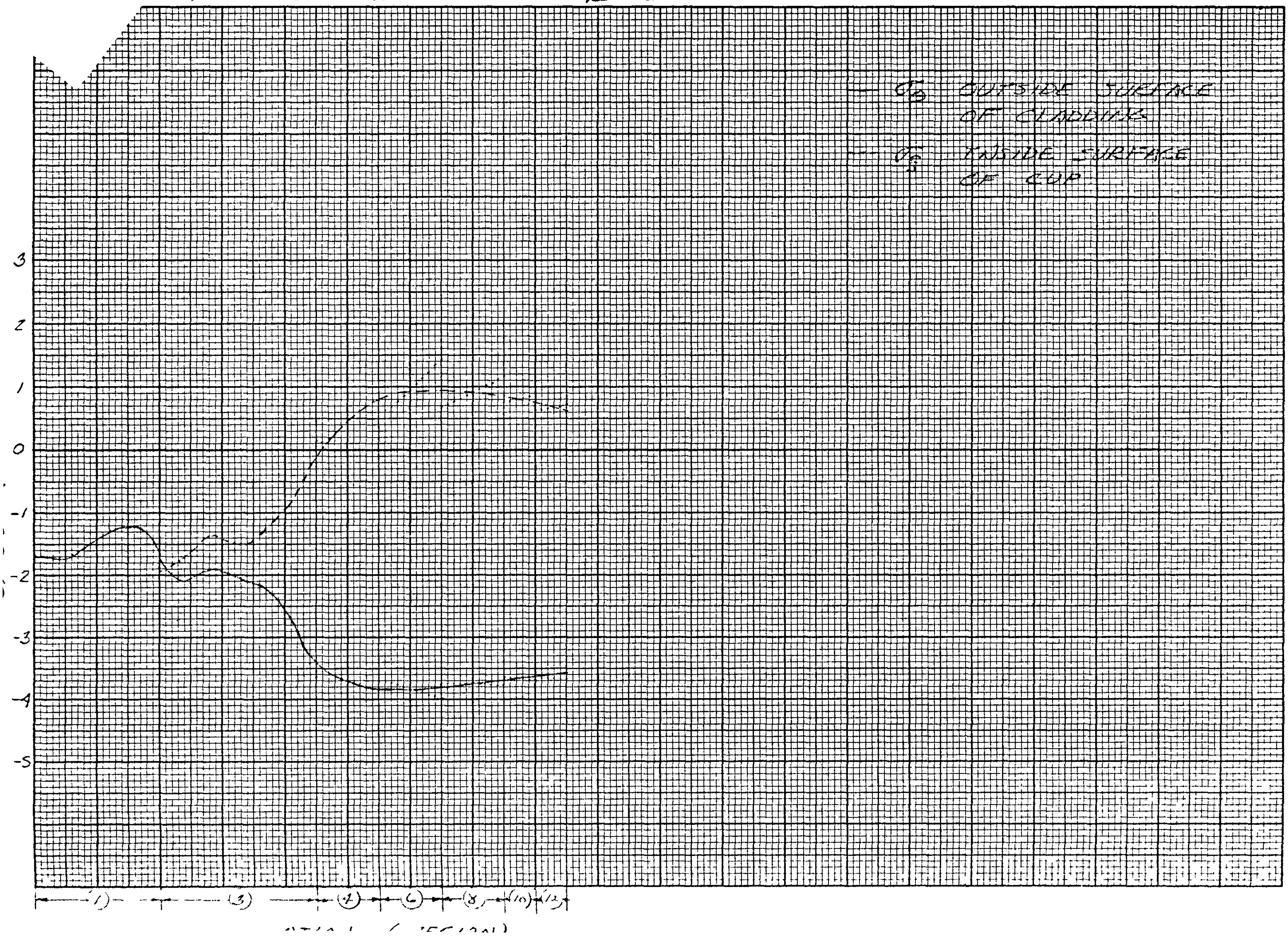

FIG. V.E.1.2.
REPRESENTATIVE METAL STRESSES-38DS LWR END CAP~ REF DESIGN - LOSS OF HEAT REJECT TRANSIENT

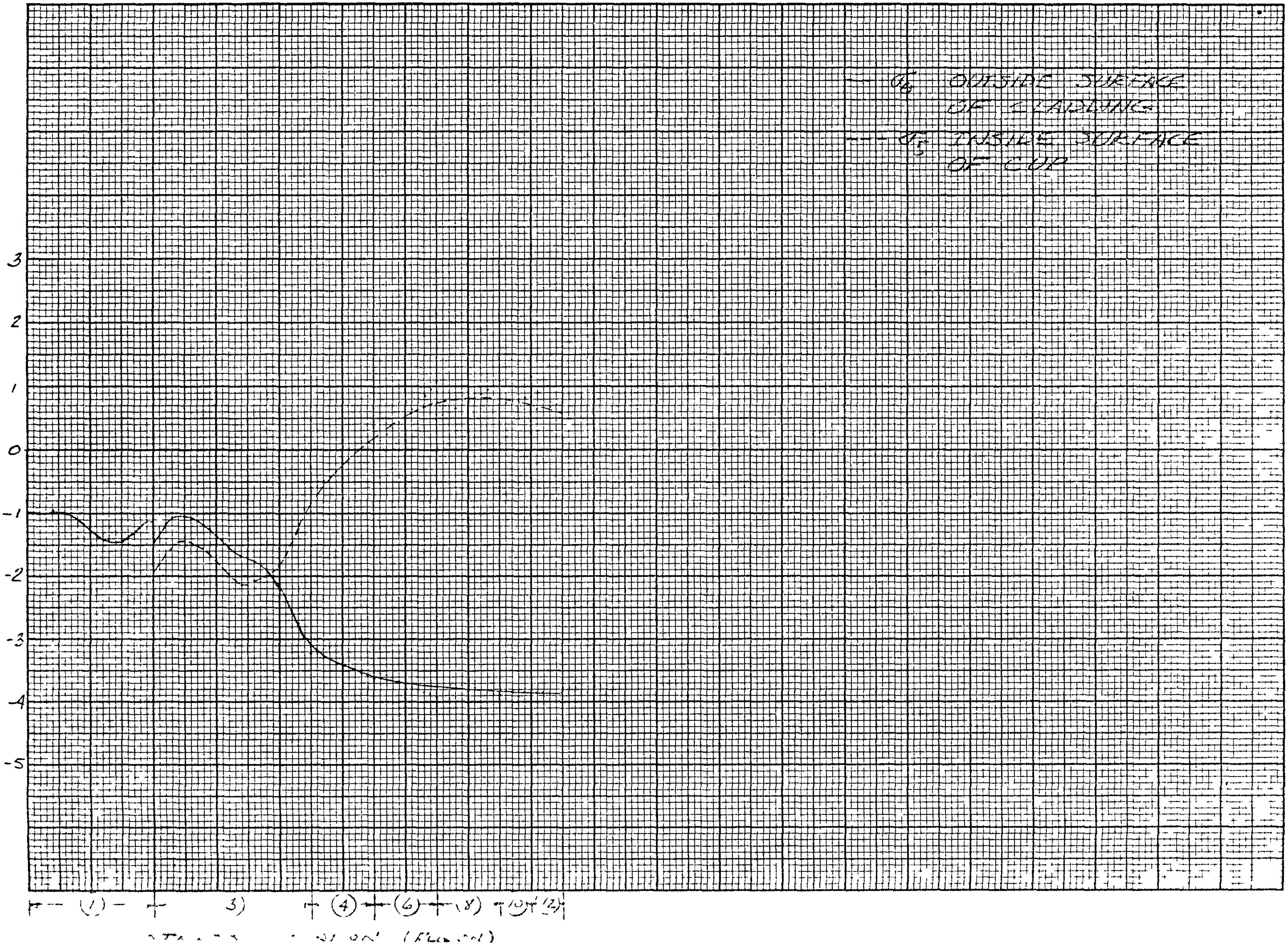

FIG. V.E 13.
REPRESENTATIVE METAL STRESSES — S8DS LWR END CAP — REF DESIGN — +200 F ISOTHERMAL

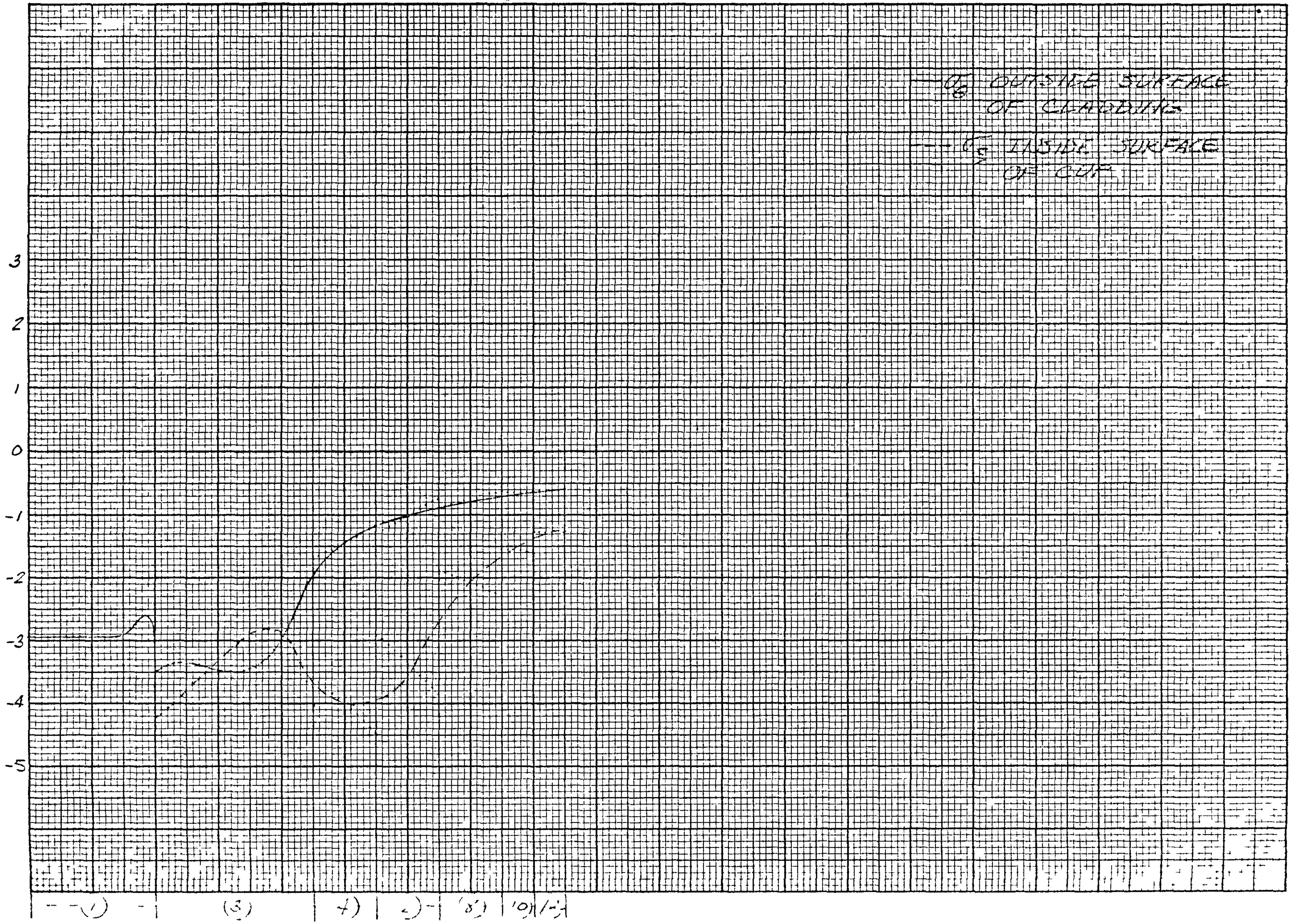

2. Upper End Cap

The maximum and minimum stresses in the upper end cap are summarized for each of the important thermal transients in Table V.E.2.1.

Stress distribution plots are presented in Figures V.E.2.1, V.E.2.2, V.E.2.3, and V.E.2.4. The solid curves represent the circumferential stresses for the outside surface of the cladding. The dashed curves represent the meridional stresses on the inner surface of the cladding. The other two principal stresses have not been plotted since they do not include the maximum and minimum values for the transients.

In general, the comments made concerning the lower end cap transient stresses are also pertinent to the upper end cap stresses.

TABLE V.E.2.1

Upper End Cap Maximum and Minimum Transient Thermal Stresses

Operating Condition	Maximum and Minimum Stresses (psi)	
	Cladding	Barrier
Isothermal @ Room Temp.	+ 27,600 (4) - 10,860 (2)	- 82,560 (4) - 97,060 (2)
200°F Cold Slug Transient	+ 1,350 (1) - 2,470 (1)	0 @ t = 0 - 3,090 (3)
200°F Hot Slug Transient	+ 2,470 (1) - 1,350 (1)	+ 3,090 (3) 0 @ t = 0
Low Flow Scram Transient	+ 3,710 (1) - 1,810 (3)	+ 4,760 (3) 0 @ t = 0
Power Scram Transient	+ 5,870 @ 12 sec (3) - 5,820 @ 6 sec (1)	0 @ t = 0 -18,300 (2) @ 12 sec
+ 200°F Isothermal	+ 1,530 (2) - 6,000 (4)	+ 21,240 (2) + 17,950 (4)

Numbers in circles ◯ denote region number for stress locations (see Figure V.A.2.)

FIG. V.E.2.1.
REPRESENTATIVE METAL STRESSES - 38DS UPPER END CAP - 200F HOT SLUG TRANSIENT

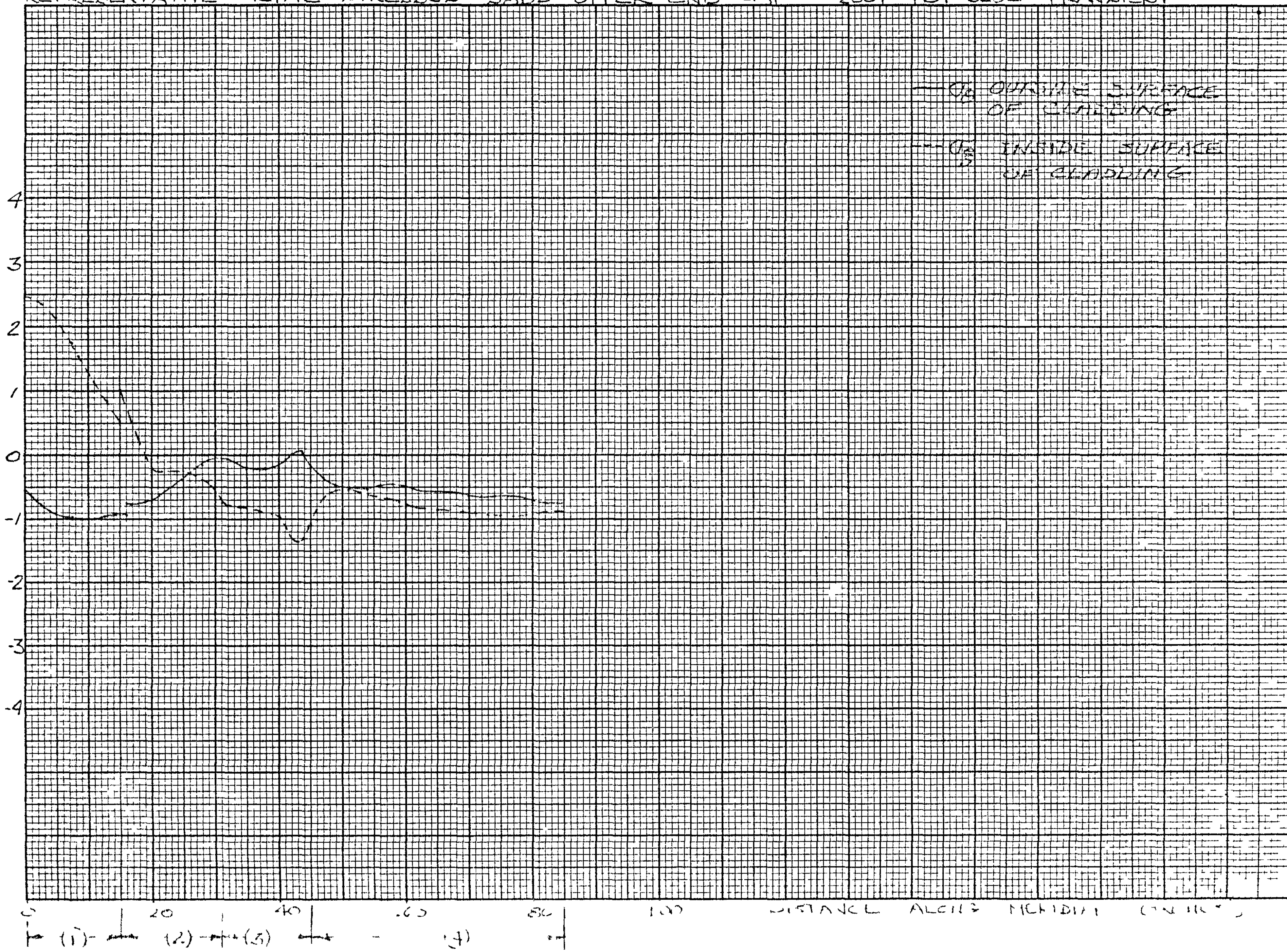

K+E 10 X 10 TO THE 1/2 INCH 359-11
KEUFFEL & ESSER CO MADE IN U.S.A.

FIG. V.E. 2.2.
REPRESENTATIVE METAL STRESSES - 58DS UPPER END CAP - LOW FLOW SCRAM TRANSIENT

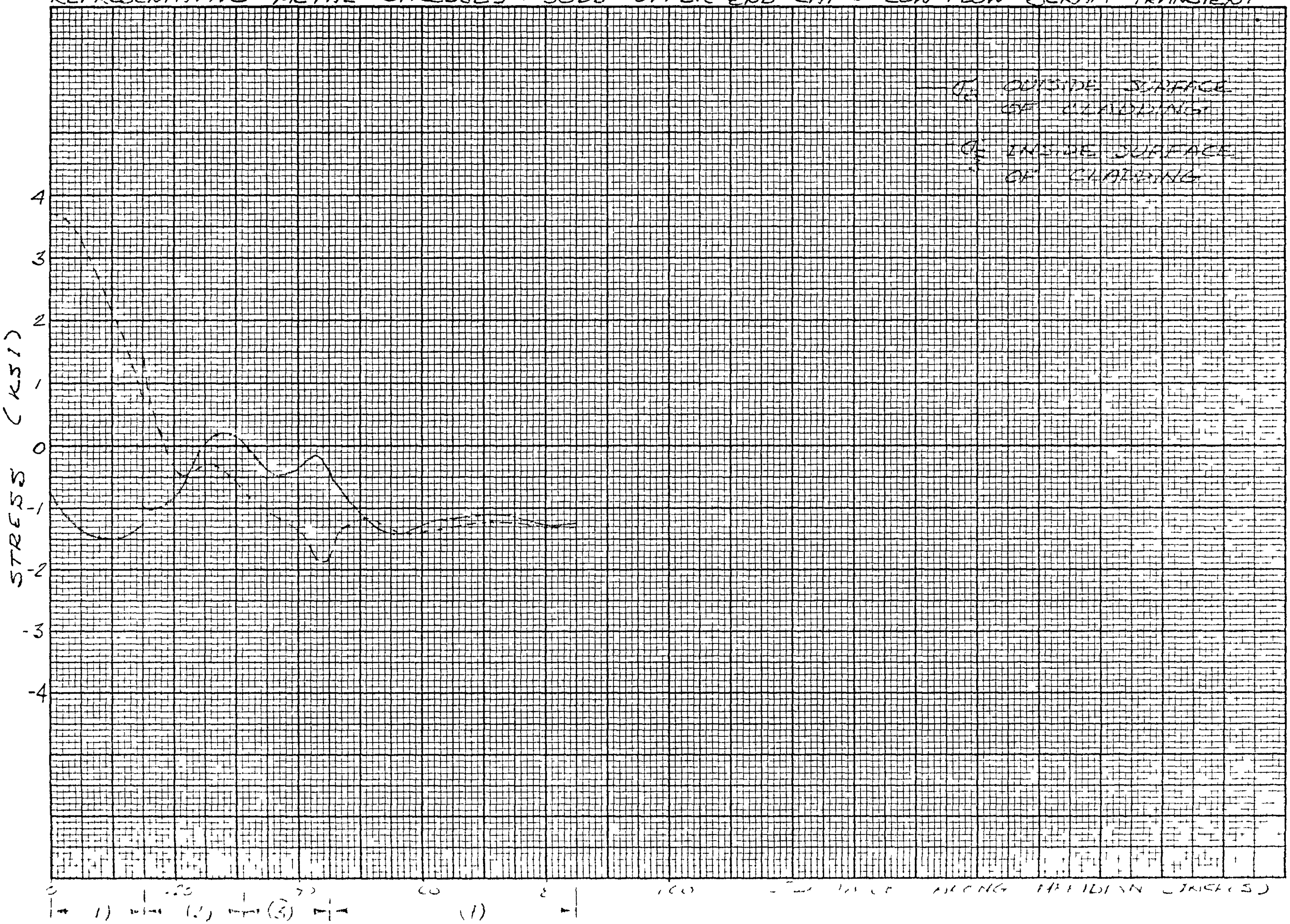

A.W.T.

FIG. V E 2 3

REPRESENTATIVE METAL STRESSES - S8DS UPPER END CAP - POWER SCRAM TRANSIENT @ t = 12 sec.

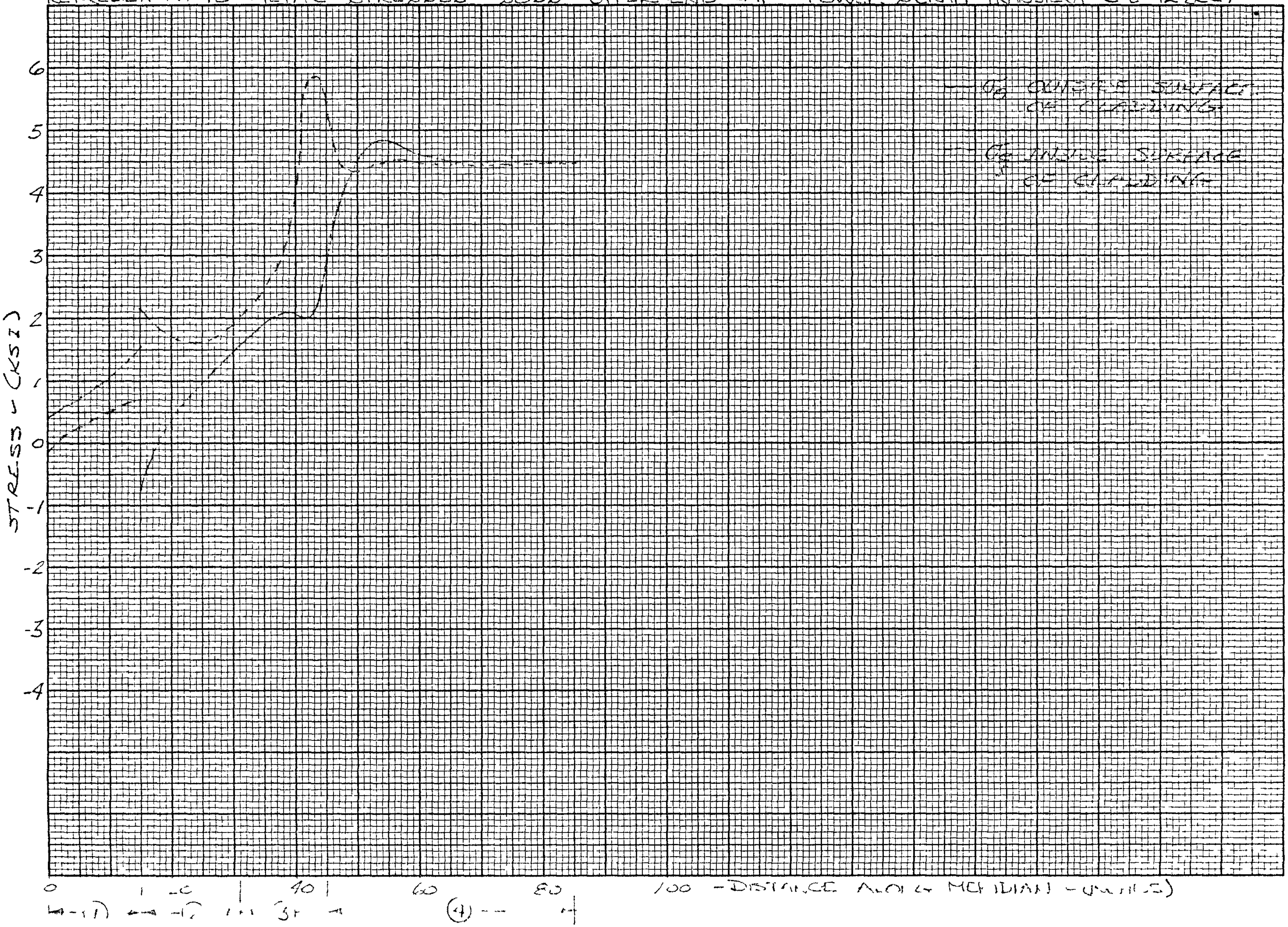

FIG. V E.2.4.
REPRESENTATIVE METAL STRESSES - 38DS UPPER END CAP - +200 F ISOTHERMAL

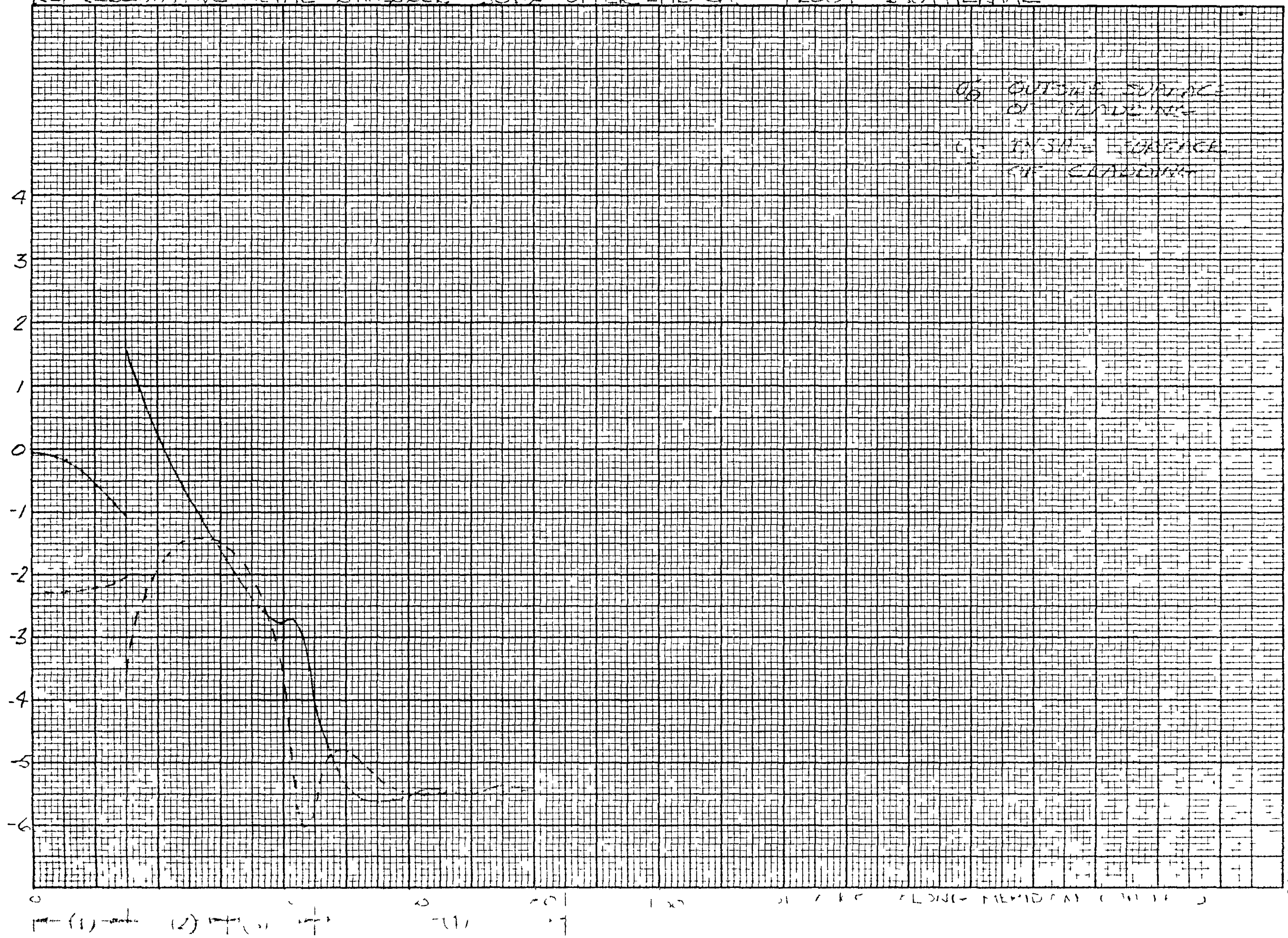

VI. EVALUATION OF RESULTS

The stresses calculated for the fuel element were evaluated in accordance with the procedures outlined in Section III of the ASME Boiler and Pressure Vessel Code (Ref. VI.1). The stresses were classified into the categories of primary (P_m, P_b, P_L), secondary (Q) and peak (F) as recommended in Article IV of the noted reference. The conditions, and identifying classification are noted in Table VI.1. Certain stresses do not fall into established categories. These were classified as 'special' and were separately evaluated.

A. Primary Stresses

The stresses are found from V.A. and V.B. and are identical for all portions of the cladding. There are no significant local membrane or primary bending stresses. The general membrane stresses during operation are:

$$\left.\begin{aligned} \sigma_Z &= -440 \\ \sigma_\theta &= -890 \\ \sigma_r &= -30 \\ \tau_{\theta Z} &= 220 \\ \tau_{\theta r} &= 430 \\ \tau_{Zr} &= 230 \end{aligned}\right\} \text{Outer Surface}$$

$$\left.\begin{aligned} \sigma_Z &= -440 \\ \sigma_\theta &= -890 \\ \sigma_r &= 0 \\ \tau_{\theta Z} &= 220 \\ \tau_{\theta r} &= 450 \\ \tau_{Zr} &= 220 \end{aligned}\right\} \text{Inner Surface}$$

TABLE VI.1
STRESS CLASSIFICATIONS
(Sheet 1 of 2)

I. Lower End Cap

1.	Ceramic coating-induced	(F)
2.	Chromizing-induced	(F)
3.	Shrink-fit residual	(F)
4.	Hydrogen-permeation-test pressure primary	(P_m)
5.	Operational pressure primary	(P_m)
6.	Hydrogen-permeation-test pressure secondary	(Q)
7.	Operational pressure secondary	(Q)
8.	Over-temp (V.B.3)	(P_m)
9.	Surge pressure (V.B.4)	(P_m)
10.	Axial thermal gradient	(Q)
11.	Thermal transients (exclusive of axial gradients)	(F)

II. Central Element

1.	Ceramic-induced	(F)
2.	Chromizing-induced	(F)
3.	Fuel-clad interference:	
	a. Axial	(Q)
	b. Circumferential	(F)
4.	Element-element interference	
	a. Axial	(Q)
	b. Circumferential	(F)
5.	Hydrogen-permeation-test pressure primary	(P_m)
6.	Operational pressure primary	(P_m)
7.	Over-temp (V.B.3)	(P_m)
8.	Surge pressure (V.B.4)	(P_m)
9.	Radial thermal gradient	(F)
10.	Circumferential gradient	(F)
11.	Hot-line creep	(Special)
12.	Creep-collapse	(Special)

TABLE VI.1

Stress Classifications

(Sheet 2 of 2)

III. Upper End Cap

1.	Chromizing stress	(F)
2.	Tube sizing residual stress	(F)
3.	Ceramic-induced stress	(F)
4.	Hydrogen-permeation-test pressure primary	(P_m)
5.	Hydrogen-permeation-test pressure secondary	(Q)
6.	Operational pressure secondary	(Q)
7.	Operational pressure primary	(P_m)
8.	Over-temp (V.B.3)	(P_m)
9.	Surge pressure (V.B.4)	(P_m)
10.	Axial thermal gradient	(Q)
11.	Circumferential gradient	(F)
12.	Hot-line creep	(Special)
13.	Creep-collapse	(Special
14.	Thermal transients (exclusive of axial gradients)	(F)

The primary stress intensity obtained from these values is

$$S = \sigma_1 - \sigma_3 = 890 \text{ psi}$$

From Section IV,

$$S_m = 3000 \text{ psi}$$

The design margin is found to be

$$\text{M.S.} = \left[\frac{3000}{890} - 1\right] 100 = +238\%$$

for primary stresses during operation.

The primary stresses during hydrogen permeation testing are:

$$\left.\begin{aligned} \sigma_Z &= +600 \\ \sigma_\theta &= +1190 \\ \sigma_r &= 0 \\ \tau_{\theta Z} &= 300 \\ \tau_{\theta r} &= 600 \\ \tau_{Zr} &= 300 \end{aligned}\right] \text{— Outer surface}$$

$$\left.\begin{aligned} \sigma_Z &= +600 \\ \sigma_\theta &= +1190 \\ \sigma_r &= -45 \\ \tau_{\theta Z} &= 300 \\ \tau_{\theta r} &= 620 \\ \tau_{Zr} &= 320 \end{aligned}\right] \text{— Inner surface}$$

From these values, the stress intensity is

$$S = 1240 \text{ psi}$$

The design margin is

$$M.S. = \left[\frac{3000}{1240} - 1\right] 100 = +142\%$$

for primary stresses during permeation testing.

In the event of fuel over-temperature, as discussed in V.B., the maximum allowable temperature without excessive cladding deformation may be determined.

The maximum stress intensity will be

$$S = (27.5\ P + P) = 28.5\ P$$

The allowable pressure is (for cladding $T_{max} = 1400^{\circ}F$)

$$P = \frac{3000}{28.5} = 105 \text{ psig}$$

With normal operating NaK pressure of 35 psi, the required hydrogen pressure becomes

$$P_H = 140 \text{ psia}$$

The minimum fuel temperature for this to occur is $1500^{\circ}F$ with H/Zr = 1.77 (Ref. VI.2). This is approximately $150^{\circ}F$ higher than the maximum fuel temperature predicted (Ref. III.B.2) (averaged axially and radially). For this calculation, the H/Zr upper limit for as-built S8DR fuel rods was used. This procedure results in the maximum dissociation pressure and the minimum margin on fuel temperature.

Should a high pressure surge occur in the NaK system, the cladding will collapse elastically at a pressure of 82 psig as noted in Section V.B. With the normal operating pressure equal to 32 psig maximum, the margin is 50 psi for this condition.

B. Secondary Stresses

Secondary stresses due to static loads are given in Sections V.A. and V.B. During hydrogen permeation testing the stresses at the upper and lower end caps are:

Outer Surface		Inner Surface	
σ_Z	-1850	σ_Z	$+1850$
σ_θ	-1560	σ_θ	-460
σ_r	0	σ_r	0
$\tau_{\theta Z}$	150	$\tau_{\theta Z}$	1160
$\tau_{\theta r}$	780	$\tau_{\theta r}$	230
τ_{Zr}	930	τ_{Zr}	930

These stresses combine with the primary stresses with the results being

Outer Surface		Inner Surface	
σ_Z	-1250	σ_Z	$+2450$
σ_θ	-370	σ_θ	$+730$
σ_r	0	σ_r	-45
$\tau_{\theta Z}$	440	$\tau_{\theta Z}$	860
$\tau_{\theta r}$	190	$\tau_{\theta r}$	390
τ_{Zr}	690	τ_{Zr}	1250

The primary plus secondary stress intensity becomes

$$S = 2500 \text{ psi}$$

The allowable stress intensity is 3 S_m (Ref. VI.1). The design margin is

$$\text{M.S.} = \left[\frac{3 \times 3000}{2500} - 1\right] 100 = +260\%$$

Secondary stresses occur in the central portion of the fuel element due to assembly interferences as summarized in Section V.A. The most critical condition is at the maximum temperature, and the stresses are

$$\left.\begin{aligned} \sigma_Z &= \pm 1600 \\ \sigma_\theta &= 0 \\ \sigma_r &= 0 \end{aligned}\right\} \text{fuel-cladding interference}$$

$$\left.\begin{aligned} \sigma_Z &= \pm 1000 \\ \sigma_\theta &= 0 \\ \sigma_r &= 0 \end{aligned}\right\} \text{element-element interference}$$

The combined secondary stresses are

$$\begin{aligned} \sigma_Z &= +2600 \quad \text{Maximum} \\ \sigma_Z &= -2600 \quad \text{Minimum} \\ \sigma_\theta &= 0 \\ \sigma_r &= 0 \end{aligned}$$

Combined with the primary stresses, during hydrogen permeation testing, the stresses become

$$\left.\begin{aligned} \sigma_Z &= +2760 \quad \text{Max} \\ \sigma_Z &= +1560 \quad \text{Min} \\ \sigma_\theta &= +1190 \\ \sigma_r &= 0 \\ \tau_{\theta Z} &= 190 \quad \text{Min} \\ \tau_{\theta Z} &= 790 \quad \text{Max} \\ \tau_{\theta r} &= 600 \\ \tau_{Zr} &= 780 \quad \text{Min} \\ \tau_{Zr} &= 1380 \quad \text{Max} \end{aligned}\right\} \text{outer surface}
\qquad
\left.\begin{aligned} \sigma_Z &= +2760 \quad \text{Max} \\ \sigma_Z &= +1560 \quad \text{Min} \\ \sigma_\theta &= +1190 \\ \sigma_r &= -45 \\ \tau_{\theta Z} &= 190 \quad \text{Min} \\ \tau_{\theta Z} &= 790 \quad \text{Max} \\ \tau_{\theta r} &= 600 \\ \tau_{Zr} &= 800 \quad \text{Min} \\ \tau_{Zr} &= 1400 \quad \text{Max} \end{aligned}\right\} \text{inner surface}$$

The maximum primary plus secondary stress intensity for the central portion of the element is

$$S = 2810 \text{ psi}$$

The design margin is

$$M.S. = \left[\frac{3 \times 3000}{2810} - 1\right] 100 = +220\%$$

during hydrogen permeation testing.

During operation, the combined primary and secondary stresses in the central portion of the element are

$\sigma_Z = +1720$	Max	outer surface	$\sigma_Z = +1720$	Max	inner surface
$\sigma_Z = -2600$	Min		$\sigma_Z = -2600$	Min	
$\sigma_\theta = -890$			$\sigma_\theta = -890$		
$\sigma_r = -30$			$\sigma_r = 0$		
$\tau_{\theta Z} = 1310$	Max		$\tau_{\theta Z} = 1310$	Max	
$\tau_{\theta Z} = 890$	Min		$\tau_{\theta Z} = 890$	Min	
$\tau_{\theta r} = 430$			$\tau_{\theta r} = 450$		
$\tau_{Zr} = 830$	Min		$\tau_{Zr} = 860$	Min	
$\tau_{Zr} = 1290$	Max		$\tau_{Zr} = 1300$	Max	

The stress intensity for this condition is

$$S = 2620 \text{ psi}$$

The margin becomes

$$M.S. = \left[\frac{3 \times 3000}{2600} - 1\right] 100 = +244\%$$

In all regions, the secondary stresses at room-temperature are small relative to the allowable room-temperature stress intensity. Design margins for these have, therefore, not been included here. These stresses have, however, been included for the evaluation of combined primary, secondary, and peak stresses.

C. Peak Stresses

Peak stresses in the lower end cap region are the results of thermal transients, ceramic coating differential expansion, chromized layer differential expansion, and residual shrink-fit pressure. The combined stresses due to the last three conditions are the following (from V.A.).

$$\left.\begin{array}{l} \left.\begin{array}{lcr} \sigma_Z & = & +\,29{,}550 \\ \sigma_\theta & = & +\,32{,}650 \\ \sigma_r & = & -\,110 \\ S_{Z\theta} & = & -\,3{,}010 \\ S_{\theta r} & = & +\,32{,}760 \\ S_{rZ} & = & -\,29{,}660 \end{array}\right] \text{inner surface} \\ \\ \left.\begin{array}{lcr} \sigma_Z & = & +\,29{,}550 \\ \sigma_\theta & = & +\,32{,}530 \\ \sigma_r & = & 0 \\ S_{Z\theta} & = & -\,2{,}980 \\ S_{\theta r} & = & +\,32{,}530 \\ S_{rZ} & = & -\,29{,}550 \end{array}\right] \text{outer surface} \end{array}\right] \text{at } 70^\circ\text{F}$$

During hydrogen permeation testing, the maximum alternating stress is found by combining the fabrication stresses and the hydrogen pressure at temperature.

$$\begin{array}{lcrlcr} \sigma_Z & = & +\,200 & S_{Z\theta} & = & -\,3180 \\ \sigma_\theta & = & +\,3380 & S_{\theta r} & = & +\,3380 \\ \sigma_r & = & 0 & S_{rZ} & = & -\,200 \end{array}$$

The maximum stress difference, establishing the alternating stress is:

$$S_{rZ} = 29,350$$

$$S_a = 14,680$$

for hydrogen permeation testing.

The stress ranges, determined in the same manner as above, for the other operating cycles, along with the alternating strain ranges, allowable number of cycles, and usage factors, are presented in Table VI.2. The table indicates that the total usage factor (U) is less than 1%.

TABLE VI.2

Lower End Cap Fatigue Stress Evaluation

Condition	n	S_a	Range	N	U
Room Temperature to Steady-State Operation	12	10,710	8.9×10^{-4}	90,000	0.013%
Steady-State to 200°F Cold Slug	25	1,430	1.2×10^{-4}	∞	-0-
Room Temperature to 200°F Hot Slug	33	12,400	1.03×10^{-3}	25,000	0.132%
Loss of Heat Reject Scram to Room Temp.	10	12,570	1.04×10^{-3}	25,000	0.040%
Hydrogen Permeation Testing	1	14,680	1.22×10^{-3}	9,000	0.011%

The number of stress cycles for each condition is derived from NAA-SR-MEMO-11373 (Ref. VI.3). For the evaluation, it was assumed that of the 55 expected startups during S8DR operation, 33 are followed by hot slugs (the total number of expected scrams) and 10 are followed by loss of heat reject scrams; leaving 12 normal startups. The 25 expected cold slugs were assumed to cycle from steady-state operating conditions. Although this assumed sequencing is unlikely in operation, it leads to the maximum cyclic stress ranges for fatigue evaluation, and it accounts for all expected transients.

The details of the stresses and stress combinations are shown in Table VI.3 and VI.4. The numbers in column headings of the former correspond to the lower end cap stress item number in Table VI.1.

Peak stresses in the central portion of the fuel result from ceramic coating differential expansion, chrome coating differential expansion, fuel-clad interference, element-element interference, and radial and circumferential thermal gradients. Stresses due to thermal transients are negligible in this region because of the extremely short response time of the cladding with the assumption that there are no local hot spots (see Section III.C.). The combined stresses, due to these conditions (from V.A, and V.C.) which produce the maximum alternating shear stress are given below. These stresses occur at the inner surface of the cladding.

$$\left.\begin{aligned}
\sigma_Z &= +\ 33{,}450\\
\sigma_\theta &= +\ 19{,}000\\
\sigma_r &= 0\\
S_{Z\theta} &= +\ 14{,}450\\
S_{\theta r} &= +\ 19{,}000\\
S_{rZ} &= -\ 33{,}450
\end{aligned}\right] \text{ at } 70^\circ\text{F}$$

$$\left.\begin{aligned}
\sigma_Z &= -\ 9{,}450\\
\sigma_\theta &= -\ 790\\
\sigma_r &= 0\\
S_{Z\theta} &= -\ 8{,}660\\
S_{\theta r} &= -\ 790\\
S_{rZ} &= +\ 9{,}450
\end{aligned}\right] \text{ at } 1200^\circ\text{F}$$

The maximum stress difference is

$$S_{rZ} = 42{,}900 \text{ psi}$$

TABLE VI.3
LOWER END CAP REGION - STRESS COMBINATIONS

	1	2	3	4	5	6	7	8	9	10	11	12	13	14	15	16	17	18	19	20
		① (70 F)	① (1400F)	① (1100 F)	② (70F)	② (1100F) (1400F)	③ (70F)	③ 1100F	③ 1400F	④ 1400F ONLY	⑥ 1400F ONLY	⑤ 1100F	⑦ 1100F	12A 200 F HOT SLUG FROM 1100	12B 200 F COLD SLUG FRIM 1100	12C LOSS OF HEAT REJ FROM 1100	12D +200F ISOTH.	12E -200F ISOTH		
1	σ_{zo} (o)	+31000	—	+8500	-1450	+1450	—	—	—	+600	-1850	-440	+1490	-3370	+3370	-2420	-2470	+2470		
2	$\sigma_{\theta o}$ (o)	+31000	—	+8500	-1450	+1450	+2980	+2450	+2300	+1190	-1560	-890	+1260	-3850	+3850	-3850	-1440	-1440		
3	σ_{ro} (o)	—	—	—	—	—	—	—	—	—	—	-30	—	—	—	—	—	—		
4	$S_{z\theta}$														-480					
5	$S_{\theta r}$														+3850					
6	S_{rz}														-3370					
7																				
8																				
9																				
10																				
11	σ_{zi} (o)	+31000	—	+8500	-1450	+1450	—	—	—	+600	+1850	-440	-1490	-2590	+2590	-2080	-2980	+2980		
12	$\sigma_{\theta i}$ (o)	+31000	—	+8500	-1450	+1450	+3100	+2550	+2390	+1190	-460	-890	+380	-3380	+3380	-3720	-1590	+1590		
13	σ_{ri} (o)	—	—	—	—	—	-110	-90	-80	—	—	—	—	—	—	—	—	—		
14	$S_{z\theta}$														-790					
15	$S_{\theta r}$														+3380					
16	S_{rz}														-2590					

PROJECT
SHEET OF

ATOMICS INTERNATIONAL
A Division of North American Aviation, Inc.

ORIGINATED BY
CALCULATED BY
CHECKED BY
DATE

FORM N 79-Y

TABLE VI.4
LOWER END CAP REGION - STRESS COMBINATIONS & STRESS RANGES

	1	2	3	4	5	6	7	8	9	10	11
		A B C (70F) ①+②+③	A (1400) ①+②+③ +④+⑥	B (1100) ①+②+③ +⑤+⑦	CA (1100) B (1100) + 12A	CC (1100) B (1100) + 12C	ΔA A - A (400) (70)	ΔB B - B (1100) (70)	ΔCA. CA - C (1100) (70)	ΔCB 12B	ΔCC CC - C (1100) (70)
1	σ_{zo} (o)	+29550	+200	+11000	+7630	+8580					
2	$\sigma_{\theta o}$ (o)	+32530	+3380	+12090	+8290	+8240					
3	σ_{ro} (o)	—	—	-30	-30	—					
4	$S_{z\theta}$	-2980	-3180	-1090	-610	+340	200	1890	2370	480	3320
5	$S_{\theta r}$	+32530	+3380	+12120	+8270	+8240	29150	20910	29260	3850	24290
6	S_{rz}	-29550	-200	-11030	-7660	-8580	29350	18520	21890	3370	20970
7											
8											
9											
10											
11	σ_{zi} (o)	+29550	+200	+11000	+8410	+8920					
12	$\sigma_{\theta i}$ (o)	+32650	+4570	+11280	+7900	+7560					
13	σ_{ri} (o)	-110	-130	-60	-60	-60					
14	$S_{z\theta}$	-3010	-4370	-280	+510	+1360	1360	2730	2500	790	4370
15	$S_{\theta r}$	+32760	+4700	+11340	+7960	+7620	28060	21420	24800	3380	25140
16	S_{rz}	-29660	-330	-10040	-8470	-8980	29330	19620	21190	2590	20680

PROJECT
SHEET
OF

NORTH AMERICAN AVIATION, INC.

CALCULATED BY
CHECKED BY
DATE

This value determines the alternating stress intensity for the central portion of the cladding

$$S_a = 21,450 \text{ psi}$$

The corresponding strain range is

$$\epsilon_{range} = \frac{2\ S_a}{E}$$

$$\epsilon_{range} = \frac{(2)(21,450)}{(24.2 \times 10^6)} = 1.78 \times 10^{-3} \text{ in./in.}$$

From Figure IV.A.2., the allowable number of cycles for this strain range is

$$N = 1800 \text{ cycles}$$

The usage factor, with n taken to be 55 cycles (Ref. VI.3.)

$$U = \frac{55}{1800} = 0.031 = 3.1\%$$

The stress range multiplier to produce failure is

$$M_\sigma = 2.7$$

The indicated design margin on stress is

$$\text{M.S.} = \left[\frac{57,800}{21,450} - 1\right] 100 = +170\%$$

As for the lower end cap, the details of the stresses and stress combinations are presented in tabular form (Tables VI.5. and VI.6.). The number headings refer to the central portion stress list numbers of Table VI.1.

TABLE VI.5
CENTRAL PORTION OF FUEL ELEMENT

	1	2	3	4	5	6	7	8	9	10	11	12	13	14	15	16	17	18	19	20
		1 (70F)	1 (1400F)	2 (70F)	2 (1400F) (1200F)	3 (70)	3 (1400)	4 (70) (1200)	5 (1400) ONLY	6 (70) (1200)	7	8	9 (1200) ONLY	10 (1200) ONLY	11	12	1 (1200F)	3 (1200F)		
1	$\sigma_{zo}(0)$	+31000	—	-1450	+1450	+4900	+1000	-1000	+600	-440			+4560	-12500			+6000	+1600		
2	$\sigma_{\theta o}(0)$	+31000	—	-1450	+1450	+11650	+2510	-1100	+1190	-890			+4560	—			+6000	+3890		
3	$\sigma_{ro}(0)$	—	—	—	—	—	—	—	—	-30			—	—			—	—		
4																				
5																				
6	$\sigma_{zo}(\pi/2)$	+31000	—	-1450	+1450	—	—	—	+600	-440			+4560	+12500			+6000	—		
7	$\sigma_{\theta o}(\pi/2)$	+31000	—	-1450	+1450	—	—	—	+1190	-890			+4560	—			+6000	—		
8	$\sigma_{ro}(\pi/2)$	—	—	—	—	—	—	—	—	-30			—	—			—	—		
9																				
10																				
11	$\sigma_{zo}(\pi)$	+31000	—	-1450	+1450	-4900	-1000	+1000	+600	-440			+4560	-12500			+6000	-1600		
12	$\sigma_{\theta o}(\pi)$	+31000	—	-1450	+1450	—	—	—	+1190	-890			+4560	—			+6000	—		
13	$\sigma_{zo}(\pi)$	—	—	—	—	—	—	—	—	-30			—	—			—	—		
14																				
15																				
16	$\sigma_{zi}(0)$	+31000	—	-1450	+1450	+4900	+1000	-1000	+600	-440			-4560	-12500			+6000	+1600		
17	$\sigma_{\theta i}(0)$	+31000	—	-1450	+1450	-11650	-2510	+1100	+1190	-890			-4560	—			+6000	-3890		
18	$\sigma_{ri}(0)$	—	—	—	—	—	—	—	-45	—			—	—			—	—		
19																				
20																				
21	$\sigma_{zi}(\pi/2)$	+31000	—	-1450	+1450	—	—	—	+600	-440			-4560	+12500			+6000	—		
22	$\sigma_{\theta i}(\pi/2)$	+31000	—	-1450	+1450	—	—	—	+1190	-890			-4560	—			+6000	—		
23	$\sigma_{ri}(\pi/2)$	—	—	—	—	—	—	—	-45	—			—	—			—	—		
24																				
25																				
26	$\sigma_{zi}(\pi)$	+31000	—	-1450	+1450	-4900	-1000	+1000	+600	-440			-4560	-12500			+6000	-1600		
27	$\sigma_{\theta i}(\pi)$	+31000	—	-1450	+1450	—	—	—	+1190	-890			-4560	—			+6000	—		
28	$\sigma_{ri}(\pi)$	—	—	—	—	—	—	—	-45	—			—	—			—	—		
29																				
30																				
31																				
32																				
33																				
34																				
35																				

PROJECT
SHEET OF

ATOMICS INTERNATIONAL
A Division of North American Aviation, Inc.

ORIGINATED BY
CALCULATED BY
CHECKED BY
DATE

FORM N 79-Y

TABLE VI.6
CENTRAL PORTION OF FUEL ELEMENT

	1	2	3	4	5	6	7	8	9	10	11	12	13	14	15	16	17	18	19	20
		E Q (70F) ①+②	E (1400F) ②+⑤	ΔE	F (1400) E+③ 1400 1400	F R (70F) E+③ (70)	ΔF	Q (1200) ①+②+⑥+⑨+⑩	ΔQ	R (1200) Q+③ 1200 1200	ΔR	S (1200) R+④ (1200)	S' (70) R+④ (70)	ΔS	T (70) Q+④ (70)(70)	T (1200) Q+⑤ (1200)(1200)	ΔT			
1	σ_{zo} (0)	+29550	+2050		+3050	+34450		-930		+670		-330	+33450		+28550	-1930				
2	$\sigma_{\theta o}$ (0)	+29550	+2640		+5150	+41200		+11120		+15010		+13910	+40100		+28450	+10020				
3	σ_{ro} (0)	–	–		–	–		-30		-30		-30	–		–	-30				
4	$S_{z\theta}$	–	-590	590	-2100	-6750	4650	-12050	12050	-14340	7590	-14240	-6650	7590	-100	-11950	11850			
5	$S_{\theta r}$	+29550	+2640	26910	+5150	+41200	36050	-11150	40700	+15040	26160	+13940	+40100	26160	+28450	+10050	18400			
6	S_{rz}	-29350	-2050	28500	-3050	-34450	31400	+900	30450	-700	33750	+300	-33450	33750	-28550	+1900	27650			
7	σ_{zo} ($\pi/2$)	+29550	+2050		+2050	+29550		+24070		+24070		+24070	+29550		+29550	+24070				
8	$\sigma_{\theta o}$ ($\pi/2$)	+29550	+2640		+2640	+29550		+11120		+11120		+11120	+29550		+29550	+11120				
9	σ_{ro} ($\pi/2$)	–	–		–	–		-30		-30		-30	–		–	-30				
10	$S_{z\theta}$	–	-590	590	-590	–	590	+12950	12950	+12950	12950	+12950	–	12950	–	+12950	12950			
11	$S_{\theta r}$	+29550	+2640	26910	+2640	+29550	26910	+11150	18400	+11150	18400	+11150	+29550	18400	+29550	+11150	18400			
12	S_{rz}	-29550	-2050	28500	-2050	-29550	27500	-24100	5450	-24100	5450	-24100	-29550	5450	-29550	-24100	5450			
13	σ_{zo} (π)	+29550	+2050		+1050	+24650		-930		-2530		-1530	+25650		+30550	-70				
14	$\sigma_{\theta o}$ (π)	+29550	+2640		+2640	+29550		+11120		+11120		+11120	+29550		+29550	+11120				
15	σ_{ro} (π)	–	–		–	–		-30		-30		-30	–		–	-30				
16	$S_{z\theta}$	–	-590	590	-590	-4900	4310	-12050	12050	-13650	8750	-12650	-3900	8750	+1000	-11190	12190			
17	$S_{\theta r}$	+29550	+2690	26910	+2640	+29550	26910	+11150	18400	+11090	18460	+11150	+29550	18400	+29550	+11150	18400			
18	S_{rz}	-29550	-2050	28500	-1050	-24650	23600	+900	30450	+2500	27150	+1500	-25650	27150	-30550	+40	30590			
19	σ_{zi} (0)	+29550	+2050		+3050	+34450		-10050		-8450		-9450	+33450		+28550	-11050				
20	$\sigma_{\theta i}$ (0)	+29550	+2640		+130	+17900		+2000		-1890		-790	+19000		+30650	+3100				
21	σ_{ri} (0)	–	-45		-45	–		–		–		–	–		–	–				
22	$S_{z\theta}$	–	-590	590	+2920	+16550	13630	-12050	12050	-6560	23110	-8660	+14450	23110	-2100	-14150	12050			
23	$S_{\theta r}$	+29550	+2690	26860	+180	+17900	17720	+2000	27550	-1890	19790	-790	+19000	19790	+30650	+3100	27550			
24	S_{rz}	-29550	-2100	28450	-3100	-34450	31350	+10050	39600	+8450	42900	+9450	-33450	42900	-28550	+11050	39600			
25	σ_{zi} ($\pi/2$)	+29550	+2050		+2050	+29550		+14950		+14950		+14950	+29550		+29550	+14950				
26	$\sigma_{\theta i}$ ($\pi/2$)	+29550	+2640		+2640	+29550		+2000		+2000		+2000	+29550		+29550	+2000				
27	σ_{ri} ($\pi/2$)	–	-45		-45	–		–		–		–	–		–	–				
28	$S_{z\theta}$ ($\pi/2$)	–	-590	590	-590	–	590	+12950	12950	+12950	12950	+12950	–	12950	–	+12950	12950			
29	$S_{\theta r}$	+29550	+2690	26860	+2690	+29550	26860	+2000	27550	+2000	27550	+2000	+29550	27550	+29550	+2000	27550			
30	S_{rz}	-29550	-2100	28540	-2100	-29550	27450	-14950	14600	-14950	14600	-14950	-29550	14600	-29550	-14950	14600			
31	σ_{zi} (π)	+29550	+2050		+1050	+24650		-10050		-11650		-10650	+25650		+30550	-9050				
32	$\sigma_{\theta i}$ (π)	+29550	+2640		+2640	+29550		+2000		+2000		+2000	+29550		+29550	+2000				
33	σ_{ri} (π)	–	-45		-45	–		–		–		–	–		–	–				
34	$S_{z\theta}$	–	-590	590	-590	-4900	5490	-12050	12050	-13650	8750	-12650	-3900	8750	+1000	-7050	8050			
35	$S_{\theta r}$	+29550	+2690	26860	+2690	+29550	26860	+2000	27550	+2000	27550	+2000	+29550	27550	+29550	+2000	27550			
		-29550	-2100	28450	-1100	-24650	23550	+10050	39600	+11650	36300	+10650	-25650	36300	-30550	+9050	39600			

FORM 79-Y-1 FORMERLY 79-Y-1V

PROJECT
SHEET OF
NORTH AMERICAN AVIATION, INC.
CALCULATED BY
CHECKED BY
DATE

All possible stress combinations were considered in order to determine the maximum stress range. This value was then used as representative of every stress cycle. This approach is conservative, but nevertheless, leads to a generous design margin indication.

Peak stresses in the upper end cap region are produced by ceramic coating differential expansion, chrome coating differential expansion, tube sizing residual stresses, circumferential thermal gradients, and thermal transients. The stress ranges for the various operational conditions are presented in Table VI.7., along with the alternating strain ranges, allowable number of cycles, and usage factors. The total usage factor, U, is less than 1%.

The upper end cap stress details are presented in Tables VI.8. and VI.9. The stress column headings correspond to the upper end cap stress list of Table VI.1.

The number of stress cycles for each condition was determined by assuming that, of the 55 expected startups, 50 are normal, and 5 are followed by power scrams. Since the stress range produced by a low flow scram to room temperature is less severe than a steady state to room temperature transient, the low flow scram was assumed to cycle from steady state conditions followed by a cold slug. Of the 25 expected cold slugs, the remaining 7 were coupled with hot slugs. As for the lower end cap, it was assumed that every scram has an associated hot slug. The remaining 7 of 33 hot slugs were considered to cycle about the steady state operating condition. This method of evaluation produces the maximum fatigue damage while accounting for all thermal transients.

TABLE VI.7

Upper End Cap Fatigue Stress Evaluation

Condition	n	S_a	Range	N	U
Room Temperature to Steady State Operation	50	14,440	1.19×10^{-3}	11,000	0.336%
Steady State to ± 200°F Slug	7	2,470	2.0×10^{-4}	∞	0.0
Steady State to + 200°F Slug	8	1,240	1.0×10^{-4}	∞	0.0
Power Scram to Room Temperature	5	16,160	1.34×10^{-3}	5,500	0.091%
Low Flow Scram to - 200°F Slug	18	3,090	2.5×10^{-4}	∞	0.0
Hydrogen Permeation Test	1	14,910	1.23×10^{-3}	8,500	0.011%

The calculated ceramic-coating-induced stresses in Section V.A. for room temperature conditions are not identical to those calculated for the same condition in Section V.E. This results from a more conservative approach being taken in the former section (worst case tolerances, etc.). For evaluation of peak stress fatigue damage, the maximum stresses, from V.A., have been used.

For the evaluation of thermal transients, the stresses in two principal directions, meridional and circumferential, were determined from the computer analysis. The third principal stress (radial) was assumed to be zero for all cases (plane stress). These stresses were then used to determine the maximum stress intensity as defined in Reference VI.1.; twice the maximum shear stress, or the absolute value of the algebraic difference between the maximum and minimum principal stresses at a point.

TABLE VI.8
UPPER PORTION OF FUEL ELEMENT - STRESSES

	1	2	3	4	5	6	7	8	9	10	11	12	13	14	15	16	17	18	19	20
		1 (70F)	1 (1300) (1400)	2 (70F)	2 (1300F) (1400F)	3 (70F)	3 (1300F)	3 (1400)	4 (1400)	5 (1400)	6 (1300)	7 (1300)	11 (1300)	14A 200F HOT SLUG FROM 1300	14B 200F COLD SLUG FROM 1300	14C LOW FLOW SCRAM FROM 1300	14D POWER SCRAM FROM 1300	14E +200F ISOTHERM	14F -200F ISOTHERM	
1	σ_{zo} (o)	-1450	+1450	+2200	+1730	+31000	+4000	—	+600	-1850	-440	+1490	-2380	-530	+530	-730	+1180	-6000	+6000	
2	$\sigma_{\theta o}$ (o)	-1450	+1450	+2200	+1730	+31000	+4000	—	+1190	-1560	-890	+1260	—	-530	+530	-730	+1180	-5380	+5380	
3	σ_{ro} (o)	—	—	—	—	—	—	—	—	—	—	—	—	—	—	—	—	—	—	
4	$S_{z\theta}$													—	—	—		-620	+620	
5	$S_{\theta r}$													-530	+530	-730		-5380	+5380	
6	S_{rz}													+530	-530	+730		+6000	-6000	
7																				
8																				
9																				
10																				
11	σ_{zi} (o)	-1450	+1450	+2200	+1730	+31000	+4000	—	+600	+1850	-440	-1490	-2380	+2470	-2470	+3710	-5820	-4810	+4810	
12	$\sigma_{\theta i}$ (o)	-1450	+1450	+2200	+1730	+31000	+4000	—	+1190	-460	-890	+380	—	+2470	-2470	+3710	-5820	-5030	+5030	
13	σ_{ri} (o)	—	—	—	—	—	—	—	—	—	—	—	—	—	—	—	—	—	—	
14	$S_{z\theta}$													—	—	—		+180	-180	
15	$S_{\theta r}$													+2470	-2470	+3710		-5030	+5030	
16	$S_{r\theta}$													-2470	+2470	-3710		+4810	-4810	

NORTH AMERICAN AVIATION, INC.

PROJECT SHEET OF

CALCULATED BY
CHECKED BY
DATE

TABLE VI.9.
UPPER PORTION OF FUEL ELEMENT - STRESS COMBINATIONS

	1	2	3	4	5	6	7	8	9	10	11	12	13	14	15
		A B C D (70) 1+2+3	A (1400) 1+2+3 +4+5 (1400)	ΔA	B (1300) 1+2+3 +6+7	ΔB	C (1300) B + 8 (1300)	ΔC	DA B + 14A (1300)	ΔDA	ΔCB 19B	DC B + 14C (1300)	ΔDC	DD B + 14D (1300)	ΔDD
1	σ_{zo} (0)	+31750	+1930		+8230		+5850		+8440			+7500		+9410	
2	$\sigma_{\theta o}$ (0)	+31750	+2810		+7550		+7550		+7590			+7020		+8730	
3	σ_{ro} (0)	—	—		—		—		—			—		—	
4	$S_{z\theta}$	—	-880	880	+680	680	-1700	1700	+850	850	–	+480	480	+680	680
5	$S_{\theta r}$	+31750	+2810	28940	+7550	24200	+7550	24200	+7590	24160	+530	+7020	24730	+8730	23020
6	S_{rz}	-31750	-1930	29820	-8230	23520	-5850	25900	-8440	23310	-530	-7500	24250	-9410	22340
7															
8															
9															
10															
11	σ_{zi} (0)	+31750	+5630		+5250		+2870		+3900			+8960		-570	
12	$\sigma_{\theta i}$ (0)	+31750	+3910		+6670		+6670		+6110			+10380		+850	
13	σ_{ri} (0)	—	—		—		—		—			—		—	
14	$S_{z\theta}$	—	+1720	1720	-1420	1420	-3800	3800	-2210	2210	–	-1420	1420	-1420	1420
15	$S_{\theta r}$	+31750	+3910	27840	+6670	25080	+6670	25080	+6110	25640	-2470	+10380	21370	+850	30900
16	S_{rz}	-31750	-5630	26120	-5250	26500	-2870	28880	-3900	27850	+2470	-8960	22790	+570	32320

NORTH AMERICAN AVIATION, INC.

PROJECT

SHEET OF

CALCULATED BY

CHECKED BY

DATE

D. Special Conditions

For evaluation of hot-line creep strain (from Section V.C.) the maximum calculated values (Figure V.C.2.) are compared with the available strain for irradiated cladding material (Ref. IV.A.2.). From Table IV of the noted reference, the minimum available creep strain is taken to be 0.31% (Specimen 5039 R) and the average strain at failure (from all specimens) is 1.19%. The indicated margins are:

$$\text{M.S.} = \left[\frac{0.31}{0.047} - 1 \right] \times 100 = +560\% \quad \text{(minimum)}$$

$$\text{M.S.} = \left[\frac{1.19}{0.047} - 1 \right] \times 100 = \text{high} \quad \text{(average)}$$

for failure during the 12,000 hour design lifetime.

From the creep-collapse results discussed in Section V.D., the design margin for this consideration is quite high based on time. Based on stress, the margin for collapse during the S8DR design life is (from Figure V.D.3.):

$$\text{M.S.} = \left[\frac{62}{35} - 1 \right] \times 100 = +77\%$$

E. Barrier Stresses

The ceramic barrier stresses vary with the stiffness of the metal to which the glass is bonded. For this reason, the maximums occur in the region of the upper and lower end cap centerlines where the metal thickness is greatest. The stresses, as noted in Tables V.E.1.1. and V.E.2.1. are compressive at room temperature. The stresses remain compressive at all temperatures since the stress condition at the start of the transients must be added to the noted stress values. For the lower end, the additive value is - 24,500 psi and for the upper end the value is - 25,700 psi. The compressive state of stress in the ceramic is the case throughout the element because the differential expansion occurs at temperatures below the stress-free condition, and, because of the small thickness of the layer, no significant thermal gradients are realized. The ceramic could, however, experience tensile stresses if prolonged operation at an elevated temperature is followed by a large temperature increase. This condition could occur if long term operation at 1100°F were followed by a hot slug. The extent of ceramic creep at the temperatures of concern has not been established quantitatively.

The design margin for the ceramic is difficult to assess because the strength properties are not well known. The values cited in Section IV.B. show that the compressive strength is approximately 80,000 psi. This stress is exceeded only at low temperatures. Since shear failures of the ceramic at room temperature have not been reported, it has been assumed that the compressive strength is greater than the calculated stresses, and fracture will not occur.

F. Cladding Evaluation Summary

Table VI.10. summarizes the design margins calculated for all stress conditions. The margins are based on stress unless otherwise noted.

TABLE VI.10
Cladding Stress Design Margins

Stress Conditions	Design Margin (Minimum)		
	Lower End Region	Central Region	Upper End Region
Primary (P_m)	+ 142%	+ 142%	+ 142%
Primary + Secondary (P_m + Q)	+ 260%	+ 220%	+ 260%
Primary + Secondary + Peak (P_m + Q + F)	+ 360%	+ 170%	+ 260%
Hot Line Creep Strain	---	+ 560%	---
Creep Collapse	---	---	+ 79%
Fuel Over-Temperature	+ 200°F	+ 150°F	+ 200°F
System Over-Pressure	---	+ 160%	---

The effects of stress ratcheting and thermal bowing were considered for the defined operating conditions, and found to not contribute significantly to the other results.

VII. CONCLUSIONS

The primary, secondary, and thermal stresses have been calculated for the SNAP 8 DR fuel element cladding. The stress analysis has included fabrication and assembly stresses as well as test and operational stresses. These have been appraised by using the evaluation procedure and philosophy of Section III of the ASME Boiler and Pressure Vessel Code (Nuclear Vessels) where applicable. Certain special conditions; creep collapse, and hot-line creep strain, were considered as special cases. A summary of the cladding evaluation is tabulated in Section VI.F.

The largest fuel element stresses are produced at room temperature due to the differential thermal contraction of the cladding and barrier from the 1400°F stress-free condition. The maximum cladding stress calculated for this condition is well below the metal's yield strength. The maximum barrier stress, however, exceeds the assumed compressive ultimate strength of the ceramic material (see Section VI.E.). If failure of the latter were to occur, it would most likely be in the form of microcracking or crazing. Room temperature failures of this sort have not been reported which tend to indicate that the actual strength of the material is greater than that assumed in Section IV. These differential contraction stresses are reduced with increasing temperature.

The largest stresses at power are produced as the result of the 6Θ temperature variation (see Section V.C.2.) occuring at the center element midplane. This condition does not produce bowing of the element provided that the circumferential variation is symmetrical. With the assumption that the elements do not rotate, these stresses are constant at constant power.

The largest stress range calculated was found to occur at the central element midplane. The range is produced by the rise from room temperature to steady-state nominal power. Since the expected number of these cycles is small, the resulting usage factor is also small (see Section VI). The associated usage factor is, however, the largest calculated for the element.

The smallest design margin calculated, based on stress is + 79%, and is associated with creep-collapse (see Section VI.D.). The design margin for this condition based on time, however, is high.

The results of this analysis indicate that the fuel element cladding is structurally adequate for the established S8DR operating conditions.

VIII. REFERENCES

I.1. SNAP 8 Fuel Element Stress Briefing - Canoga Park, California, July 19-20, 1966, NAA-SR-MEMO-12097 (CRD)

I.2. SNAP 8 Briefing - Washington, D. C., August 15-16, 1966, NAA-SR-MEMO-12122 (CRD).

I.3. SNAP 8 Briefing to AEC - Washington, D. C., December 1, 1966, NAA-SR-MEMO-12272 (CRD).

I.4. P. M. Magee, "SNAP 8 Development Reactor (S8DR) Core Thermal and Hydraulic Performance," NAA-SR-12564, March 10, 1968 (CRD).

III.A.1. L. D. Swenson, Personal Communication

III.A.2. IL, E. H. Ottewitte to H. Rood, "Comments on SNAP Fuel Element Gas Gap Conductivity," July 26, 1967.

III.A.3. L. D. Swenson, "S8DR Core Performance Evaluation," NAA-SR-12482, August 9, 1967.

III.B.1. P. M. Magee, "Detailed Thermal Analysis of SNAP Reactor Fuel Elements Including Asymmetry and Spacing Effects," NAA-SR-MEMO-12384, March 20, 1967 (CRD).

III.B.2. P. M. Magee, "SNAP 8 Development Reactor (S8DR) Core Thermal and Hydraulic Performance," NAA-SR-12564, March 10, 1968 (CRD).

III.C.1. IL, R. E. Stanbridge to R. A. Johnson, "Thermal Analysis of S8DR Fuel Elements with Alternate End Cap Designs," October 24, 1967.

IV.A.1. IL, J. P. Thorel to E. J. Donovan, "Hastelloy-N Data Report," October 27, 1966.

IV.A.2. G. G. Allaria, "ORR S-2 Irradiated Hastelloy-N Biaxial Stress-Rupture Data," NAA-SR-TDR-12457, May 2, 1967.

IV.A.3. S. S. Manson and Gary Halford, "A Method of Estimating High Temperature Low Cycle Fatigue Behavior of Materials, NASA-TMX-52270.

IV.A.4. D. G. Mason, "SNAP 8 Progress Report, May-July 1967," NAA-SR-12521, September 15, 1967 (CRD).

IV.A.5. A. W. Dalcher, "Computed Stress-Relaxation Curves for Hastelloy Alloy N," NAA-SR-TDR-12590

IV.B.1. D. F. Atkins, Unpublished thermal expansion plots for barrier materials.

IV.B.2. W. D. Kingery, "Factors Affecting Thermal Stress Resistance of Ceramic Materials," Journal of the American Ceramic Society, Vol. 38, No. 1, pp. 3-17.

V.A.1. D. T. McClelland, K. Langrod, C. A. Martin, "Process Flow Sheets, S8DR Cladding Tube Fabrication," Rev. 1., May 18, 1967 (CRD).

V.A.2. AI Spec ST0622NA0040

V.A.3. AI Spec ST0622NA0041

V.A.4. G. W. Meyers, Personal Communication

V.A.5. J. V. Facha, "Tolerance Study and Calculation of Fabrication and Assembly Stresses," July 1966 (Unpublished).

V.B.1. IL, P. M. Magee to R. A. Johnson, "Revised Rupture Temperature for S8DR Fuel Elements," July 11, 1967.

V.C.1. S. Timoshenko and S. Woinowsky-Krieger, Theory of Plates and Shells, McGraw Hill Book Co.

V.C.2. IL, P. Y. Hsieh to R. I. Jetter, "Thermal Stress and Displacement Analysis - S8ER Cladding," November 29, 1965 (CRD).

V.C.3. R. D. Elliott, Digital computer code CREEP, and CREEP problem runs, May 1967 (Undocumented).

V.D.1. Y. S. Pan, "Creep Buckling of a Thin-Walled Circular Cylindrical Shell Subject to Uniform External Pressure and Arbitrary Temperature Gradients," Presented at the 6th Annual NAA Science Symposium, Ojai, California, October 1967.

V.D.2. Letter, R. F. Wilson to Mr. J. V. Levy, Manager CPAO USAEC, "Margin of Safety on Creep Collapse of SNAP 8 Fuel Element Cladding," 67AT-2657, May 15, 1967.

V.E.1. L. Stone, Personal Communication

V.E.2. W. M. Faust, "Modification of the AVCO Program," Rocketdyne SR-4111-7001, July 23, 1964.

V.E.3. G. O. Warren to Those Listed, "Changes to the AVCO Shell Program," SSM7109-3011, August 22, 1967 (Rocketdyne).

VI.1. ASME Boiler and Pressure Vessel Code, Section III, Nuclear Vessels, 1965.

VI.2. Dissociation Pressure Isochores of Zirconium Hydride, AI Photo Plate No. 7569-01653, August 14, 1964.

VI.3. J. Roecker, "SNAP 8 Development Reactor (S8DR) Safety Analysis Report, Addendum 1," NAA-SR-MEMO-11373, P. 26.

IX. NOMENCLATURE AND SIGN CONVENTION

$\sigma_\xi = \sigma_Z$ = Longitudinal (meridional) stress component, psi

σ_θ = Tangential (circumferential) stress component, psi

σ_r = Radial stress component, psi

$\tau_{\theta Z} = \tau_{Z\theta}$ = Shearing stress component acting on the θ or Z plane in the Z or θ direction, psi

$\tau_{\theta r} = \tau_{r\theta}$ = Shearing stress component acting on the θ or r plane in the r or θ direction, psi

$\tau_{Zr} = \tau_{rZ}$ = Shearing stress component acting on the Z or r plane in the r or z direction, psi

P = Pressure, psi

r = Mean radius of cylinder, inches

t = Shell thickness, inches

Z = Axial distance along cylinder, inches (Z = 0 at lower end cap)

L = Length of cylinder, inches

ϵ_Z = Longitudinal (meridional) strain component, in./in.

ϵ_θ = Tangential (circumferential) strain component, in./in.

ϵ_r = Radial strain component, in./in.

T = Temperature, $^\circ$F

ν = Poisson's ratio

N = Number of cycles (allowable)

n = Number of cycles (operational)

$S_{Z\theta}$ = $\sigma_Z - \sigma_\theta$, stress difference, psi

$S_{\theta r}$ = $\sigma_\theta - \sigma_r$, stress difference, psi

S_{rZ} = $\sigma_r - \sigma_Z$, stress difference, psi

Δ = Increment

θ = Angle (circumferential)

U = Fatigue usage factor (= n/N)

$\bar{\alpha}$, α_i = Mean and instantaneous thermal expansion coefficients, micro inches/inch/$^\circ$F

E = Young's Modulus, psi

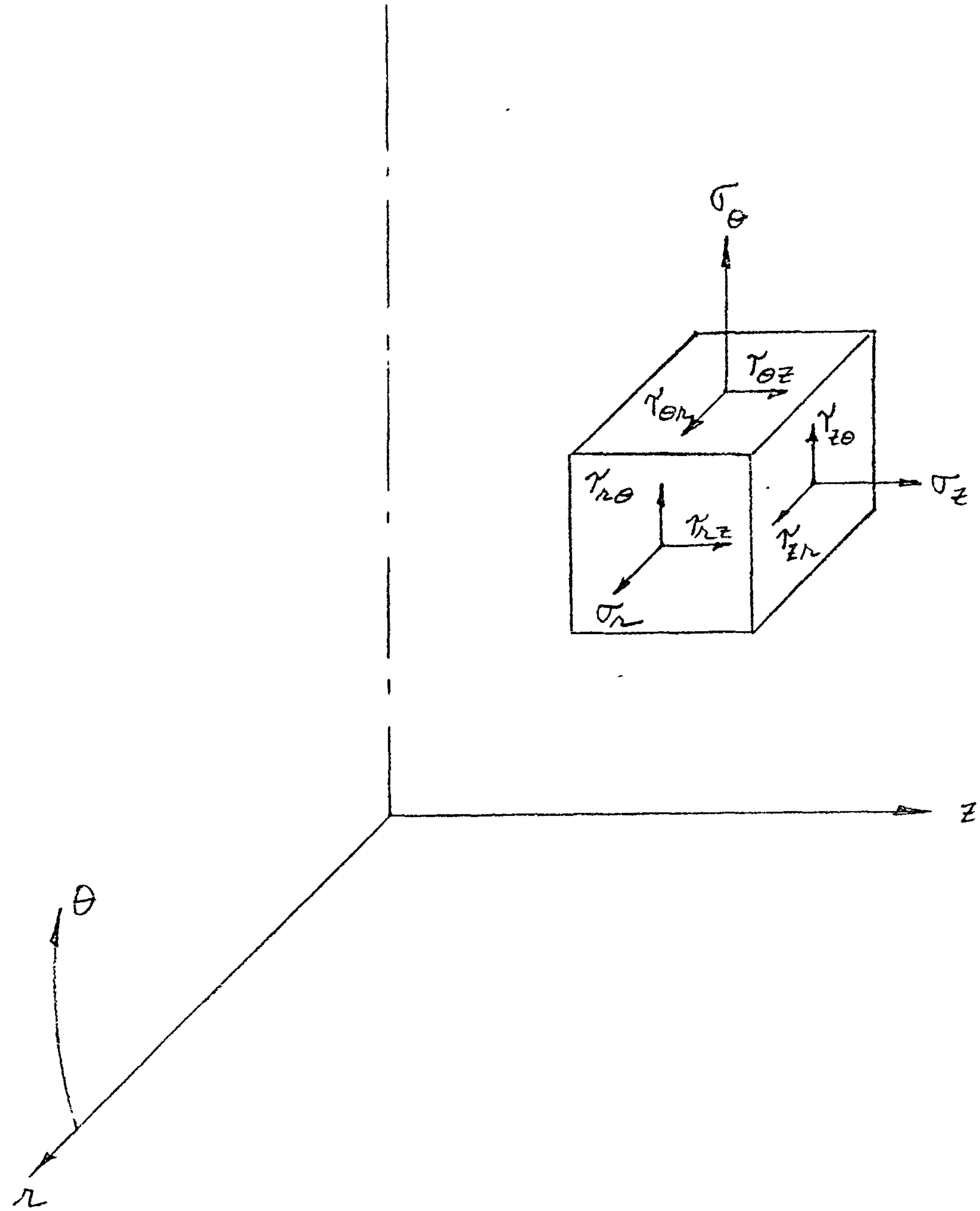

FIGURE IX.1. SIGN CONVENTION FOR STRESS COMPONENTS
THE DIRECTIONS SHOWN ARE POSITIVE.